Mesoscale convective systems modulated by convectively coupled equatorial waves

Yuan-Ming Cheng[1], Juliana Dias[1], George Kiladis[2], Zhe Feng[3], and L. Ruby Leung[4]

[1]NOAA Physical Sciences Laboratory
[2]National Oceanic and Atmospheric Administration (NOAA)
[3]Pacific Northwest National Laboratory (DOE)
[4]PNNL

March 6, 2023

Abstract

Mesoscale convective systems (MCSs) produce over 50% of tropical precipitation and account for the majority of extreme rainfall and flooding events. MCSs are considered the building blocks of larger-scale convectively coupled equatorial waves (CCEWs). While CCEWs can provide favorable environments for convection, how CCEWs can systematically impact organized convection and thereby MCS characteristics is less clear. We examine this question by analyzing a global MCS tracking dataset. During the active phase of CCEWs, MCS frequency increases and MCSs rain harder, produce more lifetime total rain, and grow larger in size. The probability of extreme MCSs also elevates. These changes are most pronounced when MCSs are associated with Kelvin waves and tropical depression-type waves while least so with the Madden-Julian Oscillation. These results can be benchmarks to improve model representation of MCS interactions with large-scale circulations and can be leveraged operationally for extended forecasts of high-impact MCSs.

Mesoscale convective systems modulated by convectively coupled equatorial waves

Yuan-Ming Cheng[1], Juliana Dias[1], George Kiladis[1], Zhe Feng[2], L. Ruby Leung[2]

[1]NOAA/Physical Sciences Laboratory, Boulder, Colorado
[2]Atmospheric Sciences and Global Change Division, Pacific Northwest National Laboratory, Richland, Washington

Key Points:

- Mesoscale convective system (MCS) frequency increases during the active phase of convectively coupled equatorial waves (CCEWs).
- MCSs tend to rain harder, produce more lifetime total rain, and grow larger in size when they occur during the active phase of CCEWs.
- The probability of extreme MCSs rises during active CCEWs. This provides an opportunity for extended forecasts of extreme rainfall events.

Corresponding author: Yuan-Ming Cheng, yuan-ming.cheng@noaa.gov

Abstract

Mesoscale convective systems (MCSs) produce over 50% of tropical precipitation and account for the majority of extreme rainfall and flooding events. MCSs are considered the building blocks of larger-scale convectively coupled equatorial waves (CCEWs). While CCEWs can provide favorable environments for convection, how CCEWs can systematically impact organized convection and thereby MCS characteristics is less clear. We examine this question by analyzing a global MCS tracking dataset. During the active phase of CCEWs, MCS frequency increases and MCSs rain harder, produce more lifetime total rain, and grow larger in size. The probability of extreme MCSs also elevates. These changes are most pronounced when MCSs are associated with Kelvin waves and tropical depression-type waves while least so with the Madden-Julian Oscillation. These results can be benchmarks to improve model representation of MCS interactions with large-scale circulations and can be leveraged operationally for extended forecasts of high-impact MCSs.

Plain Language Summary

Satellite observations show that the population of tropical clouds tends to cluster in a variety of sizes. A type of cluster with a size of around 100 km, known as mesoscale convective systems (MCSs), produces over 50% of tropical rainfall and often causes extreme rainfall and flooding events because MCSs can produce heavy rainfall for a long duration. Other larger clusters spanning from 1000 to 10000 km, such as convectively coupled equatorial waves (CCEWs), can favor the formation of convection within them. However, how CCEWs can systematically change MCS development and characteristics is not well understood. We examine this by analyzing an MCS tracking dataset. When MCSs occur within CCEWs, their frequency increases and they rain harder, produce more lifetime total rain, and grow larger in size. The probability of extreme MCSs is also elevated. These changes are most pronounced when MCSs occur within two types of CCEWs, Kelvin waves and tropical depression-type waves while least so with another, the Madden-Julian Oscillation. These results can be benchmarks to improve computer simulations of MCS interactions with large-scale circulations. Because CCEWs are better predicted than MCSs beyond one week, results here can also be leveraged operationally for forecasts of high-impact MCSs.

1 Introduction

Satellite observations of clouds in the tropics reveal a hierarchy of organized cloud clusters ranging from the planetary-scale Madden–Julian Oscillation (MJO), through synoptic-scale convectively coupled equatorial waves (CCEWs), to mesoscale convective systems (MCSs, Nakazawa, 1988; Mapes & Houze, 1993; S. S. Chen et al., 1996). These various types of convective organization are not necessarily independent from one another and MCSs, with scales of 100s of kilometers, are often considered building blocks of those larger-scale tropical circulations (Mapes et al., 2006). The most intense MCSs often cause high-impact weather events and the frequency of these rainfall extremes has increased in the past few decades and is projected to rise with climate change (Z. Feng et al., 2016; Taylor et al., 2017; Tabari, 2020; R. S. Schumacher & Rasmussen, 2020). While MCSs are difficult to predict in current global weather and climate models due to their smaller scales and dependence on subgrid-scale processes, larger-scale disturbances such as CCEWs can be predicted with higher skill beyond one week (Ying & Zhang, 2017; Dias et al., 2018; Janiga et al., 2018; Judt, 2020). Therefore, synoptic disturbances can be useful sources of extended predictability for tropical rainfall events associated with MCSs. A critical step towards this is to establish an observational understanding of how MCS characteristics and their extremes can be related to those large-scale disturbances.

The potential modulation of MCSs by large-scale tropical circulations is somewhat expected considering that 100 years of MCS research invariantly highlights how environmental conditions can impact the initiation, development, and intensity of MCSs over a wide range of climate regimes (e.g., Houze, 2018; Rotunno et al., 1988; LeMone et al., 1998; Laing & Fritsch, 2000). Vertical wind shear can favor convective cells to organize into coherent mesoscale entities. Moisture and entrainment of dry air can impact the ability of convective elements to grow upscale into extensive stratiform regions characteristics of mature MCSs (C. Schumacher & Houze, 2006; X. Chen et al., 2022). The most intense and high-impact MCSs are often a result of interactions across scales generating favorable environments for long-lasting convection (Vizy & Cook, 2022; R. S. Schumacher & Johnson, 2005; Taylor et al., 2017; Latos et al., 2021; Baranowski et al., 2020).

While the term CCEWs is traditionally reserved for convectively coupled Matsuno modes (Matsuno, 1966; Kiladis et al., 2009), here we adopt a broad perspective (Wolding et al., 2020), which also includes the MJO (Madden & Julian, 1971) and tropical depression (TD)-type disturbances or easterly waves (Takayabu & Nitta, 1993; Kiladis et al., 2006). CCEWs can modulate tropical environments to favor convective initiation and organization (Kiladis et al., 2009; Serra et al., 2020). This modulation can impact the ensemble of cloud populations and change the likelihood of MCS occurrence (Mapes et al., 2006; Yasunaga & Mapes, 2011b, 2011a; Nakamura & Takayabu, 2022a, 2022b). In addition, since the structures of CCEWs vary systematically from one another, this influences the ability of different CCEWs to support convection and determines whether groups of convective cells can develop upscale into MCSs. A recently developed 19-year MCS tracking dataset from Z. Feng et al. (2021) offers a unique opportunity to systematically examine the relationship between CCEWs and embedded MCSs across the global tropics.

The goal of this study is to document how MCSs are systematically modulated by CCEWs as part of a broad community effort to further our understanding of convective organization and wave-convection coupling in the tropics. In particular, we address two questions: 1) How do CCEWs modulate MCS frequency, characteristics, and extremes? 2) How does this modulation vary with different CCEWs? This observed relationship between organized convection and large-scale circulations can be benchmarks to improve model representations of MCS interactions with large-scale circulations and provide operational guidance for high-impact MCS events at extended lead times.

2 Data and Method

2.1 CCEW identification

We use the rainfall product of Global Precipitation Mission Integrated Multi-satellitE Retrievals for Global precipitation measurement (GPM IMERG, Huffman et al., 2020) from 2001 to 2019. The IMERG rainfall is utilized at 3-hour intervals and interpolated to 2.5 ° × 2.5 °. To identify CCEWs, tropical rainfall is filtered in wavenumber-frequency space following the standard method from M. Wheeler and Kiladis (1999), with the same parameters as in Dias et al. (2017) for Matsuno's modes and the MJO. For TDs, we apply the same filter as in Kiladis et al. (2006). Due to the large seasonal and regional variation of CCEW activity across the globe (M. Wheeler & Kiladis, 1999; Roundy & Frank, 2004; P. Huang & Huang, 2011; Dias & Kiladis, 2014), amplitudes of the filtered signals are normalized by standard deviation at each grid point using the 3-hourly data with the first three harmonics of seasonal cycle removed. In the interest of conciseness, but still considering seasonal cycles of CCEWs, we present results from March–August for Kelvin waves, June—November for TDs and mixed Rossby gravity waves (MRGs), and November–April for equatorial Rossby waves (ERs) and the MJO. These are the months when each type of CCEWs is most active (not shown).

While we have investigated all CCEWs, we exclude westward and eastward inertio-gravity waves. This is because one underlying assumption is that large-scale circulations provide a relatively unchanged environment within the typical lifetime of MCSs. The lack of scale separation between MCSs and inertio-gravity waves invalidates this assumption.

2.2 MCS database

We use the global MCS database from Z. Feng et al. (2021) where MCSs are tracked hourly from 2001 to 2019 using NASA brightness temperature (T_b) (Janowiak et al., 2017) and precipitation features (PFs) retrieved from the GPM IMERG precipitation product at 0.1° spatial resolution. The two datasets allow for more accurate identification of MCSs where their lifetime evolution and internal structure (such as convective and stratiform features manifested as rain rates) are considered. Briefly, an MCS is identified if the following criteria are met for longer than four hours (see Z. Feng et al. (2021) for more details). 1) A cold cloud system defined in T_b exceeds an area of 4×10^4 km^2 and contains at least a PF in IMERG with a major axis length larger than 100 km. 2) The PF area, mean rain rate, rain rate skewness, and heavy rain volume ratio are larger than corresponding lifetime-dependent thresholds. MCSs in the tropics are tracked in two domains and stitched together. The two domains are combined by allowing MCSs to track from east to west but not in the opposite direction near the boundaries (30°–50°E and 180°). As a result, MCS tracks in those regions need to be interpreted with caution. Only MCSs within 15°N/S are analyzed.

2.3 MCS characteristics

In the MCS dataset, each cold cloud system has hourly centroid latitudes and longitudes. These values are averaged across the MCS lifetime to obtain a mean location and time of that MCS. If the corresponding amplitude of a CCEW, measured by the nearest grid points to the mean MCS location and the closest 3-hourly time stamp to the average MCS time, is equal to or larger than one standard deviation, the MCS is determined to be concurrent with that active CCEW. Note that since tropical convection is organized at various time scales, an MCS can be associated with more than one type of active CCEWs.

We calculate five representative characteristics of MCSs to assess their intensity, sizes, and duration. The three intensity metrics are lifetime total rain, average rain rate, and maximum rain rate. The lifetime total rain is the integrated amount of rain, expressed in millimeters (mm), falling underneath an MCS cloud shield throughout its lifetime. This metric can be converted to volumetric rain in kilograms. The average rain rate, measured in mm hr^{-1}, is the mean rain rate of the largest 3 PFs of an MCS throughout its lifetime. Three PFs are used because the MCS tracking dataset only includes precipitation statistics from the largest 3 PFs, which on average produce over 70% of the lifetime total precipitation. The maximum rain rate, expressed in mm hr^{-1}, is defined as the heaviest precipitating pixel within the cloud shield during the lifetime of an MCS. The size of an MCS is expressed in km^2 as the mean area of the cold cloud shield during its lifetime. The duration is the total hours of each tracked cold cloud system. Every MCS has one value for each of these metrics to represent its overall characteristics.

We bin MCSs into 5° × 5° grid boxes. Values of MCS characteristics are standardized by the mean and standard deviation of all MCSs occurring in the same grid box and months. Despite tremendous MCS variability globally and seasonally (Houze et al., 2015; X. Huang et al., 2018; Schiro et al., 2020; Z. Feng et al., 2021), using this dimensionless Z-score in probability distribution functions (pdfs) renders distributions of MCS characteristics similar across the globe (not shown). The choice of grid-box sizes is made because the area of an individual MCS is at least 2° × 2° and this binning yields robust

statistical analysis. Tests reveal that the size of the grids does not qualitatively impact the results.

2.4 MCS frequency and risk ratio for extreme MCSs

Two ratios are defined to assess the change in MCS frequency attributable to CCEWs relative to the climatology. A frequency ratio for MCS occurrence R_{freq} in each grid box is defined as,

$$R_{freq} = \frac{\mathrm{MCS}_{wave}/\mathrm{t}_{wave}}{\mathrm{MCS}_{all}/\mathrm{t}_{all}} \tag{1}$$

MCS_{wave} is the number of MCSs concurrent with a particular CCEW, and t_{wave} is the number of times when that CCEW is active. MCS_{all} is the total number of MCSs, and t_{all} is the total number of times. For each CCEW type, all numbers are calculated for the respective 6-month periods considered from 2001 to 2019. The numerator of R_{freq} describes the frequency of MCSs when that CCEW is active and the denominator is the climatological frequency of MCSs. Taken together, R_{freq} measures the MCS frequency change associated with that CCEW normalized by climatology. A value larger than one indicates the presence of the CCEW increases the frequency of MCSs.

Similarly, we define a risk ratio to measure the frequency change of extreme MCSs. The threshold for extreme MCSs is defined as the top 10 percentile at each grid box for each 6-month period, so the climatological probability of an extreme MCS is 10%. The extremes are calculated for each of the five MCS characteristics. We define the risk ratio R_{risk} at each location as,

$$R_{risk} = \frac{\text{Extreme } \mathrm{MCS}_{wave}/\mathrm{MCS}_{wave}}{10\%}. \tag{2}$$

Extreme MCS_{wave} denotes the number of extreme MCSs concurrent with a particular CCEW. "Extreme MCS_{wave}" is normalized by the counts of MCSs concurrent with the CCEW because different waves modulate the MCS occurrence differently. The numerator as a whole calculates the probability of an MCS being categorized as extreme out of all the MCSs associated with that particular CCEW. A value of R_{risk} larger than one shows that the CCEW elevates the probability of extreme MCSs relative to a climatological value of 10%.

3 Climatological and CCEW-modulated MCS frequency

The distribution of MCS occurrence (colors in Fig. 1a) closely follows the mean tropical precipitation (contours). The frequency of MCSs is highest along the Intertropical Convergence Zone (ITCZ) where the annual precipitation is high. This correspondence between MCS counts and rainfall holds true for different seasons such that the MCS counts closely follow the migration of the ITCZ (Fig. S1). Nonetheless, the MCS occurrence does not solely depend on the mean precipitation. Landmasses, regardless of continents or islands, accumulate the highest counts of MCSs, although these regions generally show less annual rainfall than the adjacent ocean. Given that the percentage of MCS rainfall remains similar at 50–70% across the tropics (Fig 10 of Z. Feng et al., 2021), the high number of MCSs over land suggests that they produce less lifetime total rain than the oceanic ones (see also Fig. S3). Over the ocean, MCSs are most frequent over the warm pool and South Pacific Convergence Zone, as well as along the ITCZ in the Western Hemisphere. This global distribution is consistent with studies using various tracking algorithms on different satellite products (Houze et al., 2015; X. Huang et al., 2018) and reaffirms the validity of the MCS database.

Figure 1b-1d shows an increase in the MCS frequency associated with active CCEWs, as indicated by R_{freq} larger than 1 (red shading). This increase in frequency is consistent with the interpretation that convective envelopes of CCEWs favor upscale growth

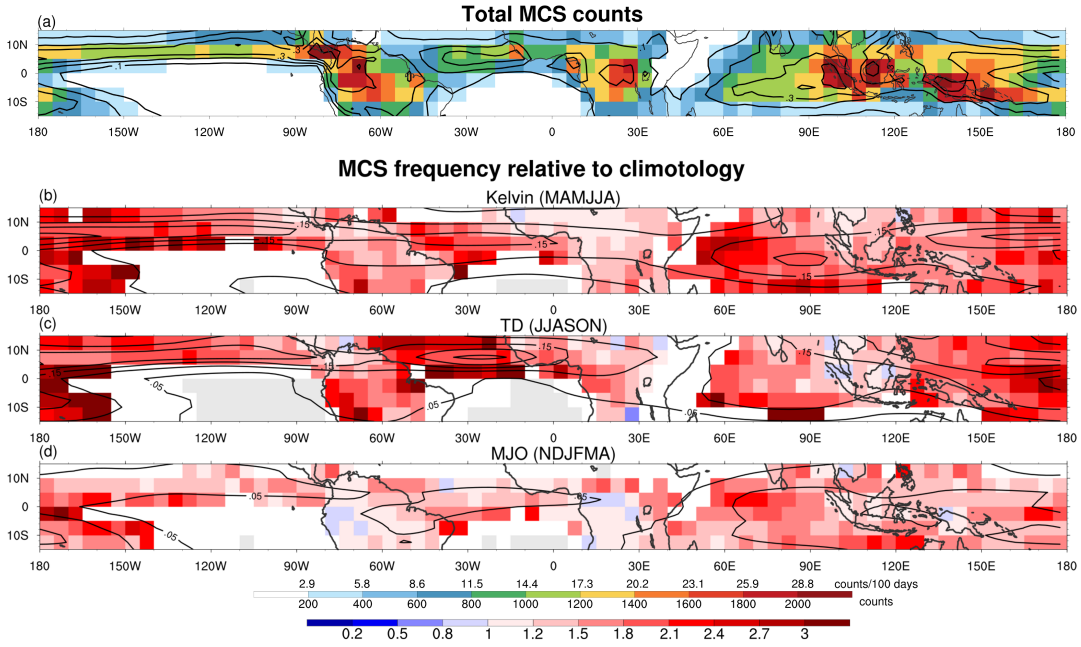

Figure 1. (a) MCS counts binned in 5° × 5° grid boxes from 2001 to 2019. Each MCS is binned by its average lifetime location. Annual mean precipitation is contoured at 0.1 mm hr^{-1}. (b)-(d) Frequency ratio (R_{freq}, colors) of MCS occurrence relative to climatology when the calculation is conditioned on (b) Kelvin waves in MAMJJA, (c) TDs in JJASON, and (d) the MJO in NDJFMA. The mean standard deviation of wave-filtered rainfall in the respective months is contoured every 0.05 mm hr^{-1} with zero lines omitted.

of convection, support the development of MCS, and thereby increase the MCS frequency. This modulation is stronger over the ocean for all CCEWs (also Fig. S2). The average R_{freq} for Kelvin waves, TDs, and the MJO over the ocean is 2.0, 2.2, and 1.6 compared to 1.4, 1.5, and 1.3 over the land. The lack of other forcing mechanisms over the ocean, such as the diurnal cycle and topography (Sakaeda et al., 2020), likely renders CCEWs more effective in supporting MCSs than over land.

The darker red shadings of R_{freq} for Kelvin waves and TDs compared to the MJO (Fig. 1b-1d) indicate stronger modulation by the former two. In fact, Kelvin waves and TDs are the two most effective modulators, followed by MRGs and ERs, and trailed by the MJO (Fig. S2). While numerous studies have highlighted the MJO as an important modulator of tropical rainfall and extreme events (e.g., Jones et al., 2004; Grimm, 2019; Schreck III, 2021; Vasconcelos Junior et al., 2021), these results suggest that synoptic-scale CCEWs influence convective organization and precipitation even more strongly than the MJO (Fink & Reiner, 2003; Linden et al., 2016; Schlueter et al., 2018; Ferrett et al., 2020; Latos et al., 2021; Lubis et al., 2022).

The elevated MCS frequency (shading in Fig. 1b-1d) overall matches well with climatological CCEW activity (contours). Kelvin waves modulate MCS frequency most strongly over the Indo-Pacific warm pool and the east Pacific but less so from South America to

Africa, consistent with the activity of Kelvin waves (Roundy & Frank, 2004; P. Huang & Huang, 2011). On the contrary, TD frequency modulation is stronger over Africa and the Atlantic, as well as the Pacific. These regions are known for strong easterly wave activity during northern summer and fall (Kiladis et al., 2006; Rydbeck & Maloney, 2014; Cheng et al., 2019; T. Feng et al., 2020). Lastly, the modulation by the MJO appears stronger over the Eastern than Western Hemisphere, consistent with the MJO's strong precipitation and circulations over the warm pool (M. C. Wheeler & Hendon, 2004; Zhang, 2005). Note that wavenumber-frequency filtering cannot unambiguously identify CCEWs (Sakaeda et al., 2020; Cheng et al., 2022; Knippertz et al., 2022), so R_{freq} in regions with climatologically low wave activity should be interpreted with caution.

4 MCS characteristics and their changes associated with CCEWs

Figure 2 shows the covariability of MCS characteristics in joint pdfs. The pdf estimates are calculated by binning MCS characteristics according to their Z-scores (Sec. 2.3). In this standardized format, zeros mark the mean at each grid box and the nonzero integers indicate the number of standard deviations from the mean. To aid interpretation, physical quantities corresponding to the Z-scores in various regions are provided in Fig. S3. In all panels of Fig. 2, we choose lifetime total rain as a benchmark variable in all y-axes because 1) it is an integrated measure of MCS's socioeconomic impact as it is a function of rain rates, sizes, and duration, and 2) it is a representative metric for approximating latent heat release important for wave–convection coupling (Nakamura & Takayabu, 2022a; Chien & Kim, 2023; Rios-Berrios et al., 2023). The x-axis denotes four other MCS characteristics in each column: average rain rates, maximum rain rates, sizes, and duration (defined in Sec. 2.3).

The climatological pdfs (Fig.2a–2d) demonstrate the diverse behaviors of MCSs. For instance, MCSs with a high amount of lifetime total rain at 2 standard deviations above the mean is comprised of those with average and maximum rain rates ranging from -1 to 4 standard deviations, as well as sizes and duration from -1 to 5. The median of lifetime total rain for each bin in both intensity metrics (black dots in Fig. 2a and 2b) levels off for rain rates above 2 standard deviations. Indeed, both intensity metrics are only moderately correlated with lifetime total rain (correlation coefficients of 0.35 and 0.48). This suggests that heavy rain rates alone do not necessarily produce a high amount of lifetime total rain because heavy rain may not be sustained for a long time or cover a large area. On the contrary, lifetime total rain is strongly correlated with sizes and duration (0.72 and 0.69, Fig. 2c and 2d). This indicates that MCSs covering a large area and/or lasting for a long period of time are very likely to produce high amounts of lifetime total rain. It is worth noting that sizes and duration are only weakly correlated at 0.28 (not shown), suggesting that a large MCS is not necessarily long-lived and vice versa.

The pdfs of MCS characteristics change substantially when MCSs are conditioned on active CCEWs (bottom three rows of Fig. 2). In the first three panels for Kelvin waves (Fig. 2e–2g), the population decreases (blue shading) in the low-left corner and increases in the upper-right (red shading). This change indicates that MCSs rain harder, produce more lifetime total rain, and grow larger in size when they are concurrent with active Kelvin waves. For duration vs. lifetime total rain (Fig. 2h), the population shifts toward the upper-left corner, which suggests two related interpretations. 1) For a given duration of MCSs, those collocated with active Kelvin waves produce more rain (green vs. black dots). 2) For a given amount of lifetime total rain, the MCS duration tends to be shorter. This population change indicates that the MCSs are more "efficient" in producing the same amount of lifetime total rain, suggesting an increase in rain rates and/or sizes, consistent with Fig. 2e–2g.

Nearly identical shifts of MCS characteristics occur when TDs are active (2i–2l). For the MJO, a similar pattern change is observed but the amplitude is weaker than Kelvin

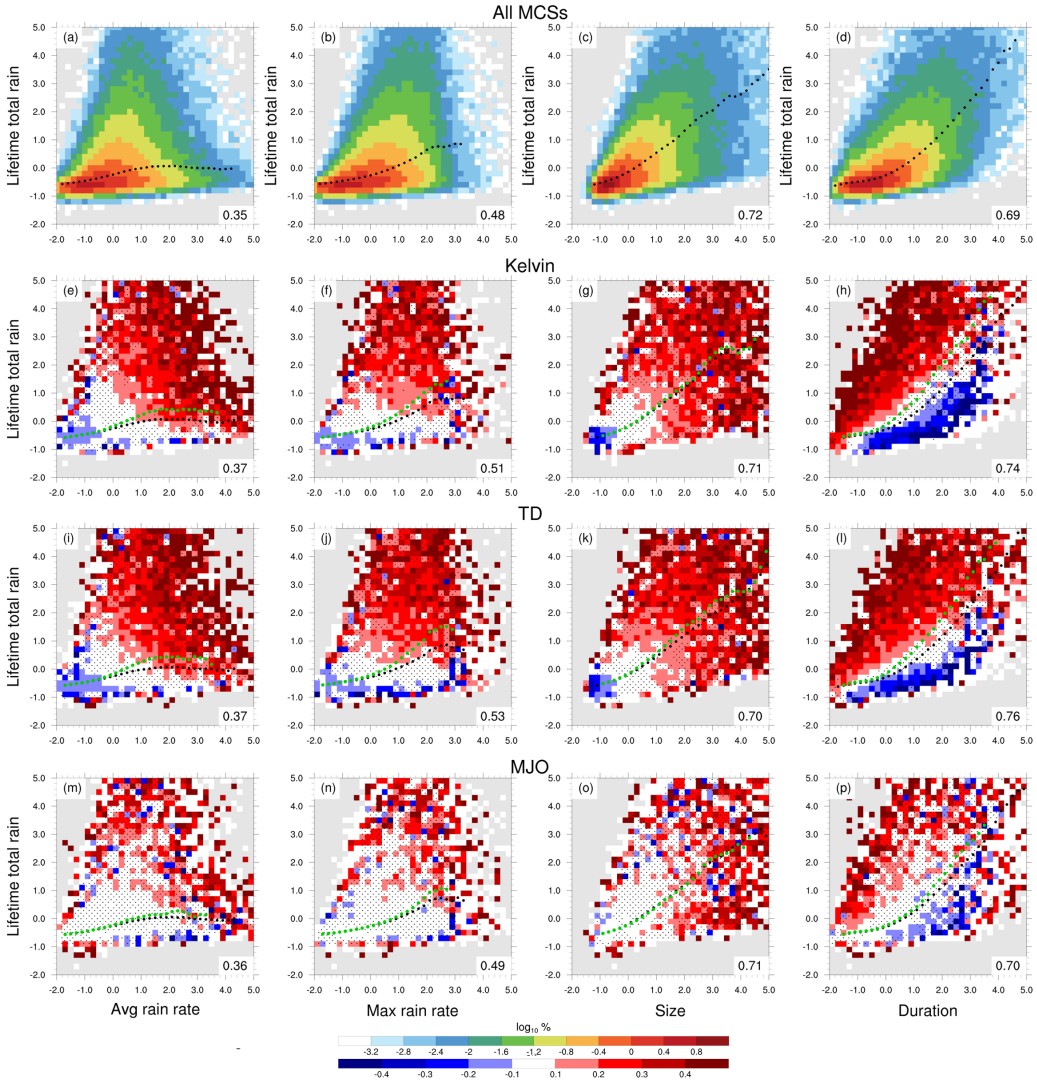

Figure 2. Top row (a–d): Joint probability distribution functions (pdfs) of MCS characteristics for all MCSs. Bottom three rows: Change of pdfs from all-MCS ones when MCSs are conditioned on (e–h) Kelvin waves, (i–l) TDs, and (m–p) the MJO. The first column shows pdfs for average rain rate vs. lifetime total rain; the second maximum rain rate vs. lifetime total rain; the third sizes vs. lifetime total rain; the fourth duration vs. lifetime total rain. In the first row, color shadings indicate the log_{10} of the percentage of total MCS counts in each bin while in the bottom three rows, colors show the log_{10} percentage change from all-MCS pdfs. Numbers on the lower-right corner of each panel denote the correlation coefficient between the two variables for all MCSs (top row) and those conditioned on CCEWs (bottom three rows). Black dots denote the median of lifetime total rain binned by the four characteristics in the x-axis for all MCSs and green dots mark the same median but for CCEW-conditioned MCSs. Stippling shows bins that are statistically *not* significant from the all-MCS pdf at the 95% interval estimated using 1000 times random sampling. Gray shading indicates bins with no MCS occurrence.

waves and TDs. Indeed, similar pattern changes occur for all CCEWs, but the amplitude of modulation differs (Fig. S4). Kelvin waves and TDs exhibit the most pronounced change in characteristics, followed by MRGs and ERs, trailed by the MJO. These systematic changes confirm that all CCEWs provide environments for MCSs to rain harder, produce more rain, and grow larger in size, although the extent of these enhancements depends on the type of CCEWs.

A natural question related to the change of characteristics is: do MCSs concurrent with active CCEWs behave differently from those without? Interestingly, the correlation among MCS characteristics, conditioned on CCEWs or not, remains remarkably similar, as shown by the correlation coefficients on the lower right corner of each panel in Figs. 2 and S4. This suggests that the change does not favor one characteristic over the other. Instead, the convective envelope of CCEWs provides a favorable environment for MCS development, but the underlying MCS dynamics likely remain similar with or without CCEWs.

5 Risks of extreme MCSs associated with CCEWs

The fact that MCSs tend to rain harder, produce more lifetime total rain, and develop into larger systems when they occur within active large-scale circulations suggests a more frequent occurrence of extreme MCSs associated with CCEWs. In this section, we investigate extreme MCSs with respect to the five characteristics used so far. Using all five metrics is because a single one cannot thoroughly depict the range of socioeconomic impacts of extreme rainfall events. For instance, extremely heavy rain rates can cause severe local flash floods while an extremely high amount of lifetime total rain can lead to widespread flooding.

The risk ratio R_{risk} measures the frequency change of extreme MCSs due to CCEWs (Sec. 2.4). Recall that a value of R_{risk} larger than one indicates that CCEWs elevate the probability of extreme MCSs relative to the climatological value of 10%. Figures 3a-3c and S5 show that CCEWs generally elevate the probability of MCSs with extremely high amounts of lifetime total rain (red colors). Kelvin waves and TDs elevate the risk by a factor of two across the majority of the tropics. Interestingly, tropical Africa shows mixed signals by Kelvin waves but a strong increase by TDs. Kelvin waves are known to modulate precipitation (Nguyen & Duvel, 2008; Mekonnen & Thorncroft, 2016; Schlueter et al., 2018, 2019) and extreme rainfall (Lafore et al., 2017; Nicholson et al., 2022) over Africa. However, Fig. 3b shows that TDs, or African easterly waves, are more strongly correlated with extreme MCS rainfall events, consistent with Vizy and Cook (2022). The MJO shows overall slight increases in probability but those increases are interspersed with decreases around the globe (Fig. 3c). The most robust increase appears over the Indian Ocean and the equatorial Maritime Continent, consistent with strong MJO signals in the region and previous studies (M. C. Wheeler & Hendon, 2004; Zhang, 2005; Da Silva & Matthews, 2021; Schreck III, 2021; Lubis et al., 2022). The mixed probability over South America and Africa is somewhat similar to the noisy signal in Schreck III (2021) but slightly at odds with Vasconcelos Junior et al. (2021) over South America, likely due to a different definition of extreme events. R_{risk} for MCSs with extreme maximum rain rates shows a remarkably similar pattern (Fig S6) to Fig. 3a–3c.

Figure 3d summarizes the global average of statistically significant R_{risk} for each of the characteristics. Kelvin waves and TDs nearly double the probabilities of extreme MCSs in all MCS characteristics (lifetime total in red, two rain intensity metrics in orange and yellow, and sizes in green) except for duration (blue). Interestingly, for both types of CCEWs, while there is slight variation in the amplitude of modulation (R_{risk} ranging from 1.7 to 1.9), the prevalence of extreme MCSs, as measured by the percentage of the global tropics showing statistically significant signals, differentiates the modulation of one characteristic from another. More than 60% of the tropics shows more fre-

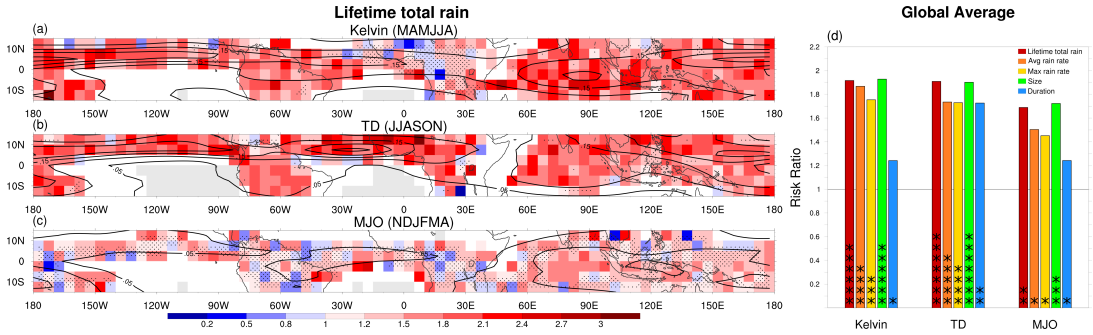

Figure 3. Risk ratio (R_{risk}) for MCSs with extremely high lifetime total rain for (a) Kelvin waves, (b) TDs, and (c) the MJO. Mean standard deviation of wave-filtered rainfall in the respective 6 months is contoured every 0.05 mm hr^{-1}. (d) Average R_{risk} for CCEWs over the global tropics where the risk ratio is statistically significant at the 95% interval. Asterisks indicate how prevalent statistically significant signals are. Each asterisk represents 10% of the grid boxes in the global tropics. In (a)–(c), stippling marks statistically *not* significant regions at the 95% interval estimated using 1000 times random sampling. Grid boxes accumulating less than 100 counts of MCSs over the 6 months during 2001–2019 are plotted white and those with no MCS occurrence gray. In (d), the legend shows different flavors of extreme MCSs in various colors.

quent extremely large MCSs and extremely high lifetime total rain, compared to only 30–50% of the tropics having extremely heavy rain rates. Similarly, the MJO elevates R_{risk} for the lifetime total rain, intensity, and sizes but to a weaker extent (R_{risk} ranging from 1.4 to 1.7) and over fewer regions (10–30% of the global tropics). The relationship between CCEWs and extreme MCSs, as measured by R_{risk} and its prevalence, is strongest for Kelvin waves and TDs, followed by MRGs and ERs, and trailed by the MJO (Fig S5, S6, and S7).

CCEWs marginally modulate the probability of extremely long-lasting systems. The R_{risk} (blue) is increased to 1.7 by TDs and to 1.2 by Kelvin waves and the MJO. Nonetheless, the areas affected by all types of CCEWs are limited to 10–20% of the tropics, much lower than other MCS characteristics. This weak modulation of extremely long-lived MCSs is consistent with the marginal impact of CCEWs on MCS duration (not shown).

6 Conclusions and Discussions

Our analysis of MCSs using satellite-derived tropical cloudiness and rainfall demonstrates that MCSs are modulated by CCEWs. More specifically, when MCSs are concurrent with active CCEWs: 1) MCSs occur more frequently (Fig. 1). 2) MCSs tend to rain harder, produce more lifetime total rain, and grow larger in size (Fig. 2). 3) The probability of extreme MCSs is elevated across a large portion of the tropics (Fig. 3). 4) These changes in MCS frequencies and characteristics are most pronounced when MCSs are associated with Kevin waves and TDs, followed by the MRGs and ERs, and trailed by the MJO.

We have also found that different MCS characteristics are modulated by CCEWs to varying degrees. While mesoscale clustering generally enhances tropical precipitation (Angulo-Umana & Kim, 2023), the interplay among physical constraints, such as moisture sources from moisture convergence and surface fluxes (Doswell et al., 1996), the energetics of ocean-atmosphere discharge-recharge cycles (S. S. Chen et al., 2016), and the extent of favorable MCS environments provided by CCEWs likely determines the am-

plitude of enhancements. Interestingly, while CCEWs may favor mesoscale convective organization, the fact that correlations among MCS characteristics are relatively insensitive to CCEWs (Fig. 2) indicates that CCEWs do not fundamentally alter MCS dynamics.

The varying strengths of MCS modulation among CCEWs are likely rooted in their differing convective coupling mechanisms (Yasunaga & Mapes, 2011b; Wolding et al., 2020; Nakamura & Takayabu, 2022b; Adames, 2022; Sakaeda & Torri, 2022). CCEWs such as the MJO and ER are primarily driven by moisture variability. Others such as Kelvin waves and African easterly waves demonstrate strong gravity wave characteristics where adiabatic motions driven by wave dynamics play a key role in convective coupling. In addition, the different convective evolution observed in Kelvin waves and ERs suggests that the stretched building block hypothesis may not explain convective coupling across all CCEWs (Nakamura & Takayabu, 2022b). These differing coupling mechanisms warrant further investigation to better understand the interactions between convective and large-scale circulations (Houze et al., 2000; Ocasio et al., 2020).

We note the following caveats of this study. Convective organization occurs across time scales (Gottschalck et al., 2013; Peatman et al., 2021) and wavenumber-frequency filtering cannot unambiguously identify CCEWs (Sakaeda et al., 2020; Cheng et al., 2022; Knippertz et al., 2022). One may argue that the stronger modulation from higher-frequency CCEWs can be attributed to MCS projection onto the wavenumber-frequency space due to comparable spatial and temporal scales. However, we have found that the amplitude of the waves is weakly correlated with MCS characteristics (not shown), suggesting that other physical mechanisms contribute to the MCS-CCEW relationship. A related caveat is the weaker modulation by the MJO. This could be the result of interference among enhanced and suppressed phases of smaller-scale CCEWs embedded in the MJO planetary-scale convective envelope (Straub & Kiladis, 2003; Roundy, 2008; Dias et al., 2013, 2017).

Our results have the following potential implications. From a model development perspective, organized convection has been poorly represented in global models with convection parameterization (Moncrieff et al., 2017) and marginally constrained in cloud-permitting models (Stevens et al., 2019). Various characteristics used here such as size and duration in observations can be utilized as benchmarks for model development. Studies have also shown that either incorporating the aggregated effects of organized convection in cumulus parameterization (Moncrieff et al., 2017; Bengtsson et al., 2021) or using cloud-resolving capabilities (Judt & Rios-Berrios, 2021; Rios-Berrios et al., 2023; Jung & Knippertz, 2023) can improve model representation of CCEWs. However, whether these models can reproduce MCS modulations by the large-scale forcing documented here needs to be investigated. In addition, the results regarding extreme MCSs suggest that forecasts of high-impact events at long lead times need to consider forecasts of CCEWs along with those of the MJO. This statistical analysis may be combined with global models to provide a probabilistic forecast of extremes at extended lead times.

Acknowledgments

YMC is grateful for the National Research Council postdoctoral research associateship at NOAA Physical Sciences Laboratory. ZF and LRL are supported by the Office of Science, U.S. Department of Energy Biological and Environmental Research as part of the Regional and Global Model Analysis program area. Pacific Northwest National Laboratory is operated for the Department of Energy by Battelle Memorial Institute under contract no. DE-AC05-76RL01830. We also thank Brandon Wolding and Stefan Tulich whose contributions helped improve the analysis and discussion.

Data Availability Statement

The GPM IMERG precipitation data can be accessed from NASA Goddard Earth Sciences Data and Information Services Center at https://doi.org/10.5067/GPM/IMERG/3B-HH/06. The global Merged IR data can be obtained from NASA Goddard Earth Sciences Data and Information Services Center at https://doi.org/10.5067/P4HZB9N27EKU. The MCS tracking algorithm is open source and detailed in Z. Feng et al. (2022).

References

Adames, A. F. (2022). The basic equations Under Weak temperature gradient balance: Formulation, scaling, and types of convectively-coupled motions. *Journal of the Atmospheric Sciences*, *-1*. doi: 10.1175/JAS-D-21-0215.1

Angulo-Umana, P., & Kim, D. (2023). Mesoscale convective clustering enhances tropical precipitation. *Science Advances*, *9*(2), eabo5317. doi: 10.1126/sciadv.abo5317

Baranowski, D. B., Flatau, M. K., Flatau, P. J., Karnawati, D., Barabasz, K., Labuz, M., ... Marzuki (2020). Social-media and newspaper reports reveal large-scale meteorological drivers of floods on Sumatra. *Nat Commun*, *11*, 2503. doi: doi.org/10.1038/s41467-020-16171-2

Bengtsson, L., Dias, J., Tulich, S., Gehne, M., & Bao, J.-W. (2021). A stochastic parameterization of organized tropical convection using cellular automata for global forecasts in NOAA's unified forecast system. *Journal of Advances in Modeling Earth Systems*, *13*(1), e2020MS002260. doi: 10.1029/2020MS002260

Chen, S. S., Houze, R. A., & Mapes, B. E. (1996). Multiscale variability of deep convection in relation to large-scale circulation in TOGA COARE. *Journal of the Atmospheric Sciences*, *53*(10), 1380–1409. doi: 10.1175/1520-0469(1996)053⟨1380:MVODCI⟩2.0.CO;2

Chen, S. S., Kerns, B. W., Guy, N., Jorgensen, D. P., Delanoë, J., Viltard, N., ... Savarin, A. (2016). Aircraft observations of dry air, the ITCZ, convective cloud systems, and cold pools in MJO during DYNAMO. *Bulletin of the American Meteorological Society*, *97*(3), 405–423. doi: 10.1175/BAMS-D-13-00196.1

Chen, X., Leung, L. R., Feng, Z., & Yang, Q. (2022). Precipitation-moisture coupling over tropical oceans: Sequential roles of shallow, deep, and mesoscale convective systems. *Geophysical Research Letters*, *49*(7), e2022GL097836. doi: 10.1029/2022GL097836

Cheng, Y.-M., Thorncroft, C. D., & Kiladis, G. N. (2019). Two Contrasting African Easterly Wave Behaviors. *J. Atmos. Sci.*, *76*, 1753–1768. doi: 10.1175/JAS-D-18-0300.1

Cheng, Y.-M., Tulich, S., Kiladis, G. N., & Dias, J. (2022). Two extratropical pathways to forcing tropical convective disturbances. *Journal of Climate*, *35*(20), 2987–3009. doi: 10.1175/JCLI-D-22-0171.1

Chien, M.-T., & Kim, D. (2023). Representation of the convectively coupled kelvin waves in modern reanalysis products. *Journal of the Atmospheric Sciences*, *80*(2), 397–418. Retrieved from `https://journals.ametsoc.org/view/journals/atsc/80/2/JAS-D-22-0067.1.xml` doi: 10.1175/JAS-D-22-0067.1

Da Silva, N. A., & Matthews, A. J. (2021). Impact of the madden–julian oscillation on extreme precipitation over the western maritime continent and southeast asia. *Quarterly Journal of the Royal Meteorological Society*, *147*(739), 3434-3453. doi: doi.org/10.1002/qj.4136

Dias, J., Gehne, M., Kiladis, G. N., Sakaeda, N., Bechtold, P., & Haiden, T. (2018). Equatorial waves and the skill of ncep and ecmwf numerical weather prediction systems. *Mon. Wea. Rev.*, *146*, 1763 - 1784. doi: 10.1175/MWR-D-17-0362.1

Dias, J., & Kiladis, G. N. (2014). Influence of the basic state zonal flow on convectively coupled equatorial waves. *Geophysical Research Letters*, 6904–6913. doi: 10.1002/2014GL061476

Dias, J., Leroux, S., Tulich, S. N., & Kiladis, G. N. (2013). How systematic is organized tropical convection within the MJO? *Geophysical Research Letters*, *40*. doi: 10.1002/grl.50308

Dias, J., Sakaeda, N., Kiladis, G. N., & Kikuchi, K. (2017). Influences of the MJO on the space-time organization of tropical convection. *Journal of Geophysical Research: Atmospheres*, *122*(15), 8012-8032. doi: doi.org/10.1002/2017JD026526

Doswell, C. A., Brooks, H. E., & Maddox, R. A. (1996). Flash flood forecasting: An ingredients-based methodology. *Weather and Forecasting*, *11*(4), 560–581. doi: 10.1175/1520-0434(1996)011⟨0560:FFFAIB⟩2.0.CO;2

Feng, T., Yang, X.-Q., Yu, J.-Y., & Huang, R. (2020). Convective coupling in tropical-depression-type waves. part i: Rainfall characteristics and moisture structure. *Journal of the Atmospheric Sciences*, *77*(10), 3407–3422. doi: 10.1175/JAS-D-19-0172.1

Feng, Z., Hardin, J., Barnes, H. C., Li, J., Leung, L. R., Varble, A., & Zhang, Z. (2022). PyFLEXTRKR: a flexible feature tracking python software for convective cloud analysis. *EGUsphere*, 1–29. doi: 10.5194/egusphere-2022-1136

Feng, Z., Leung, L. R., Hagos, S., Houze, R. A., Burleyson, C. D., & Balaguru, K. (2016, November). More frequent intense and long-lived storms dominate the springtime trend in central US rainfall. *Nature Communications*, *7*(1), 13429. doi: 10.1038/ncomms13429

Feng, Z., Leung, L. R., Liu, N., Wang, J., Houze Jr, R. A., Li, J., ... Guo, J. (2021). A global high-resolution mesoscale convective system database using satellite-derived cloud tops, surface precipitation, and tracking. *Journal of Geophysical Research: Atmospheres*, *126*(8), e2020JD034202. doi: doi.org/10.1029/2020JD034202

Ferrett, S., Yang, G.-Y., Woolnough, S. J., Methven, J., Hodges, K., & Holloway, C. E. (2020). Linking extreme precipitation in southeast asia to equatorial waves. *Quarterly Journal of the Royal Meteorological Society*, *146*(727), 665-684. doi: https://doi.org/10.1002/qj.3699

Fink, A. H., & Reiner, A. (2003). Spatiotemporal variability of the relation between African easterly waves and west African squall lines in 1998 and 1999. *J. Geophys. Res.*, *108*, 4332. doi: 10.1029/2002JD002816

Gottschalck, J., Roundy, P. E., Iii, C. J. S., Vintzileos, A., & Zhang, C. (2013). Large-scale atmospheric and oceanic conditions during the 2011–12 DYNAMO field campaign. *Monthly Weather Review*, *141*(12), 4173–4196. Retrieved from `https://journals.ametsoc.org/view/journals/mwre/141/12/mwr-d-13-00022.1.xml` doi: 10.1175/MWR-D-13-00022.1

Grimm, A. M. (2019). Madden–julian oscillation impacts on south american summer monsoon season: precipitation anomalies, extreme events, teleconnections, and role in the MJO cycle. *Clim Dyn*, *53*(1), 907–932. doi: 10.1007/s00382-019-04622-6

Houze, R. A. (2018). 100 years of research on mesoscale convective systems. *Meteorological Monographs*, *59*, 17.1 - 17.54. doi: 10.1175/AMSMONOGRAPHS-D-18-0001.1

Houze, R. A., Chen, S. S., Kingsmill, D. E., Serra, Y., & Yuter, S. E. (2000). Convection over the pacific warm pool in relation to the atmospheric kelvin-rossby wave. *Journal of the Atmospheric Sciences*, *57*(18), 3058–3089. doi: 10.1175/1520-0469(2000)057⟨3058:COTPWP⟩2.0.CO;2

Houze, R. A., Rasmussen, K. L., Zuluaga, M. D., & Brodzik, S. R. (2015). The variable nature of convection in the tropics and subtropics: A legacy of 16 years of the tropical rainfall measuring mission satellite. *Reviews of Geophysics*, *53*(3), 994-1021. doi: https://doi.org/10.1002/2015RG000488

Huang, P., & Huang, R. (2011). Climatology and interannual variability of convectively coupled equatorial waves activity. *J. Climate*, *24*(16), 4451–4465. doi:

10.1175/2011JCLI4021.1

Huang, X., Hu, C., Huang, X., Chu, Y., Tseng, Y.-h., Zhang, G. J., & Lin, Y. (2018). A long-term tropical mesoscale convective systems dataset based on a novel objective automatic tracking algorithm. *Climate Dynamics*, *51*(7), 3145–3159. doi: 10.1007/s00382-018-4071-0

Huffman, G. J., Bolvin, D. T., Braithwaite, D., Hsu, K.-L., Joyce, R. J., Kidd, C., ... Xie, P. (2020). Integrated multi-satellite retrievals for the global precipitation measurement GPM mission IMERG. In V. Levizzani, C. Kidd, D. B. Kirschbaum, C. D. Kummerow, K. Nakamura, & F. J. Turk (Eds.), *Satellite precipitation measurement: Volume 1* (pp. 343–353). Cham: Springer International Publishing. doi: 10.1007/978-3-030-24568-9_19

Janiga, M. A., Schreck, C. J., Ridout, J. A., Flatau, M., Barton, N. P., Metzger, E. J., & Reynolds, C. A. (2018). Subseasonal forecasts of convectively coupled equatorial waves and the mjo: Activity and predictive skill. *Mon. Wea. Rev.*, *146*. doi: 10.1175/MWR-D-17-0261.1

Janowiak, J., Joyce, B., & Xie, P. (2017). Ncep/cpc l3 half hourly 4km global (60s - 60n) merged ir V1 [dataset]. *Goddard Earth Sciences Data and Information Services Center (GES DISC)*. doi: 10.5067/P4HZB9N27EKU

Jones, C., Waliser, D. E., Lau, K. M., & Stern, W. (2004). Global occurrences of extreme precipitation and the madden–julian oscillation: Observations and predictability. *Journal of Climate*, *17*(23), 4575–4589. doi: 10.1175/3238.1

Judt, F. (2020). Atmospheric predictability of the tropics, middle latitudes, and polar regions explored through global storm-resolving simulations. *J. Atmos. Sci.*, *77*, 257 - 276. doi: 10.1175/JAS-D-19-0116.1

Judt, F., & Rios-Berrios, R. (2021). Resolved convection improves the representation of equatorial waves and tropical rainfall variability in a global nonhydrostatic model. *Geophysical Research Letters*, *48*(14), e2021GL093265. doi: 10.1029/2021GL093265

Jung, H., & Knippertz, P. (2023). Link between the time-space behavior of rainfall and 3d dynamical structures of equatorial waves in global convection-permitting simulations. *Geophysical Research Letters*, *50*(2), e2022GL100973. doi: 10.1029/2022GL100973

Kiladis, G. N., Thorncroft, C. D., & Hall, N. M. J. (2006). Three-Dimensional Structure and Dynamics of African Easterly Waves. Part I: Observations. *J. Atmos. Sci.*, *63*, 2212–2230. doi: 10.1175/JAS3741.1

Kiladis, G. N., Wheeler, M. C., Haertel, P. T., Straub, K. H., & Roundy, P. E. (2009). Convectively coupled equatorial waves. *Rev. Geophys.*, *47*, RG2003. doi: 10.1029/2008RG000266

Knippertz, P., Gehne, M., Kiladis, G. N., Kikuchi, K., Rasheeda Satheesh, A., Roundy, P. E., ... Wheeler, M. C. (2022). The intricacies of identifying equatorial waves. *Quarterly Journal of the Royal Meteorological Society*, *148*(747), 2814–2852. doi: 10.1002/qj.4338

Lafore, J.-P., Beucher, F., Peyrillé, P., Diongue-Niang, A., Chapelon, N., Bouniol, D., ... Vischel, T. (2017). A multi-scale analysis of the extreme rain event of ouagadougou in 2009. *Quarterly Journal of the Royal Meteorological Society*, *143*(709), 3094-3109. doi: https://doi.org/10.1002/qj.3165

Laing, A. G., & Fritsch, J. M. (2000). The large-scale environments of the global populations of mesoscale convective complexes. *Monthly Weather Review*, *128*(8), 2756–2776. doi: 10.1175/1520-0493(2000)128⟨2756:TLSEOT⟩2.0.CO;2

Latos, B., Lefort, T., Flatau, M. K., Flatau, P. J., Permana, D. S., Baranowski, D. B., ... Schmidt, J. M. (2021). Equatorial waves triggering extreme rainfall and floods in southwest sulawesi, indonesia. *Mon. Wea. Rev.*, *149*(5), 1381 - 1401. doi: 10.1175/MWR-D-20-0262.1

LeMone, M. A., Zipser, E. J., & Trier, S. B. (1998). The role of environmental shear and thermodynamic conditions in determining the structure and evolution of

mesoscale convective systems during TOGA COARE. *Journal of the Atmospheric Sciences*, *55*(23), 3493–3518. doi: 10.1175/1520-0469(1998)055⟨3493:TROESA⟩2.0.CO;2

Linden, R. v. d., Fink, A. H., Pinto, J. G., Phan-Van, T., & Kiladis, G. N. (2016). Modulation of daily rainfall in southern vietnam by the madden–julian oscillation and convectively coupled equatorial waves. *Journal of Climate*, *29*(16), 5801–5820. doi: 10.1175/JCLI-D-15-0911.1

Lubis, S. W., Hagos, S., Hermawan, E., Respati, M. R., Ridho, A., Risyanto, ... Permana, D. S. (2022). Record-breaking precipitation in indonesia's capital of jakarta in early january 2020 linked to the northerly surge, equatorial waves, and MJO. *Geophysical Research Letters*, *49*(22), e2022GL101513. doi: 10.1029/2022GL101513

Madden, R. A., & Julian, P. R. (1971). Detection of a 40–50 day oscillation in the zonal wind in the tropical pacific. *Journal of the Atmospheric Sciences*, *28*(5), 702–708. doi: 10.1175/1520-0469(1971)028⟨0702:DOADOI⟩2.0.CO;2

Mapes, B. E., & Houze, R. A. (1993). Cloud clusters and superclusters over the oceanic warm pool. *Monthly Weather Review*, *121*(5), 1398–1416. doi: 10.1175/1520-0493(1993)121⟨1398:CCASOT⟩2.0.CO;2

Mapes, B. E., Tulich, S., Lin, J., & Zuidema, P. (2006). The mesoscale convection life cycle: Building block or prototype for large-scale tropical waves? *Dynamics of Atmospheres and Oceans*, *42*(1), 3–29. doi: 10.1016/j.dynatmoce.2006.03.003

Matsuno, T. (1966). Quasi-geostrophic motions in the equatorial area. *J. Meteor. Soc. Japan*, *44*, 25-43. doi: 10.2151/jmsj1965.44.1_25

Mekonnen, A., & Thorncroft, C. D. (2016). On mechanisms that determine synoptic time scale convection over east africa. *International Journal of Climatology*, *36*(12), 4045-4057. doi: doi.org/10.1002/joc.4614

Moncrieff, M. W., Liu, C., & Bogenschutz, P. (2017). Simulation, modeling, and dynamically based parameterization of organized tropical convection for global climate models. *J. Atmos. Sci.*, *74*(5), 1363–1380. doi: 10.1175/JAS-D-16-0166.1

Nakamura, Y., & Takayabu, Y. N. (2022a). Convective couplings with equatorial rossby waves and equatorial kelvin waves. part i: Coupled wave structures. *Journal of the Atmospheric Sciences*, *79*(1), 247–262. doi: 10.1175/JAS-D-21-0080.1

Nakamura, Y., & Takayabu, Y. N. (2022b). Convective couplings with equatorial rossby waves and equatorial kelvin waves. part II: Coupled precipitation characteristics. *Journal of the Atmospheric Sciences*, *79*(11), 2919 – 2933. doi: 10.1175/JAS-D-22-0003.1

Nakazawa, T. (1988). Tropical super clusters within intraseasonal variations over the western pacific. *Journal of the Meteorological Society of Japan. Ser. II*, *66*(6), 823-839. doi: 10.2151/jmsj1965.66.6_823

Nguyen, H., & Duvel, J.-P. (2008). Synoptic wave perturbations and convective systems over equatorial africa. *Journal of Climate*, *21*(23), 6372 - 6388. doi: 10.1175/2008JCLI2409.1

Nicholson, S. E., Fink, A. H., Funk, C., Klotter, D. A., & Satheesh, A. R. (2022). Meteorological causes of the catastrophic rains of october/november 2019 in equatorial africa. *Global and Planetary Change*, *208*, 103687. doi: doi.org/10.1016/j.gloplacha.2021.103687

Ocasio, K. M. N., Evans, J. L., & Young, G. S. (2020). A wave-relative framework analysis of AEW–MCS interactions leading to tropical cyclogenesis. *Monthly Weather Review*, *148*(11), 4657–4671. doi: 10.1175/MWR-D-20-0152.1

Peatman, S. C., Schwendike, J., Birch, C. E., Marsham, J. H., Matthews, A. J., & Yang, G.-Y. (2021). A local-to-large scale view of maritime continent rainfall: Control by ENSO, MJO, and equatorial waves. *Journal of Climate*, *34*(22),

8933–8953. doi: 10.1175/JCLI-D-21-0263.1

Rios-Berrios, R., Judt, F., Bryan, G., Medeiros, B., & Wang, W. (2023). Three-dimensional structure of convectively coupled equatorial waves in aquaplanet experiments with resolved or parameterized convection. *Journal of Climate*, 1–44. doi: 10.1175/JCLI-D-22-0422.1

Rotunno, R., Klemp, J. B., & Weisman, M. L. (1988). A theory for strong, long-lived squall lines. *Journal of Atmospheric Sciences*, *45*(3), 463 - 485. doi: 10.1175/1520-0469(1988)045⟨0463:ATFSLL⟩2.0.CO;2

Roundy, P. E. (2008). Analysis of convectively coupled Kelvin waves in the Indian Ocean MJO. *J. Atmos. Sci.*, *65*, 1342–1359. doi: 10.1175/2007JAS2345.1

Roundy, P. E., & Frank, W. M. (2004). A climatology of waves in the equatorial region. *J. Atmos. Sci.*, *61*(17), 2105–2132. doi: 10.1175/1520-0469(2004)061⟨2105:ACOWIT⟩2.0.CO;2

Rydbeck, A. V., & Maloney, E. D. (2014). Energetics of east pacific easterly waves during intraseasonal events. *Journal of Climate*, *27*(20), 7603–7621. doi: 10.1175/JCLI-D-14-00211.1

Sakaeda, N., Kiladis, G., & Dias, J. (2020). The diurnal cycle of rainfall and the convectively coupled equatorial waves over the maritime continent. *Journal of Climate*, *33*(8), 3307–3331. doi: 10.1175/JCLI-D-19-0043.1

Sakaeda, N., & Torri, G. (2022). The behaviors of intraseasonal cloud organization during DYNAMO/AMIE. *Journal of Geophysical Research: Atmospheres*, *127*(7), e2021JD035749. doi: 10.1029/2021JD035749

Schiro, K. A., Sullivan, S. C., Kuo, Y.-H., Su, H., Gentine, P., Elsaesser, G. S., ... Neelin, J. D. (2020). Environmental controls on tropical mesoscale convective system precipitation intensity. *Journal of the Atmospheric Sciences*, *77*(12), 4233 - 4249. doi: 10.1175/JAS-D-20-0111.1

Schlueter, A., Fink, A. H., & Knippertz, P. (2019). A systematic comparison of tropical waves over northern Africa. Part II: Dynamics and thermodynamics. *J. Climate*. doi: 10.1175/JCLI-D-18-0651.1

Schlueter, A., Fink, A. H., Knippertz, P., & Vogel, P. (2018). A Systematic Comparison of Tropical Waves over Northern Africa. Part I: Influence on Rainfall. *J. Climate*, *32*, 1501–1523. doi: 10.1175/JCLI-D-18-0173.1

Schreck III, C. J. (2021). Global survey of the mjo and extreme precipitation. *Geophysical Research Letters*, *48*(19), e2021GL094691. doi: https://doi.org/10.1029/2021GL094691

Schumacher, C., & Houze, R. A. (2006). Stratiform precipitation production over sub-saharan africa and the tropical east atlantic as observed by TRMM. *Quarterly Journal of the Royal Meteorological Society*, *132*(620), 2235–2255. doi: 10.1256/qj.05.121

Schumacher, R. S., & Johnson, R. H. (2005). Organization and environmental properties of extreme-rain-producing mesoscale convective systems. *Monthly Weather Review*, *133*(4), 961–976. doi: 10.1175/MWR2899.1

Schumacher, R. S., & Rasmussen, K. L. (2020). The formation, character and changing nature of mesoscale convective systems. *Nature Reviews Earth & Environment*, *1*(6), 300–314. doi: 10.1038/s43017-020-0057-7

Serra, Y. L., Rowe, A., Adams, D. K., & Kiladis, G. N. (2020). Kelvin waves during goamazon and their relationship to deep convection. *Journal of the Atmospheric Sciences*, *77*(10), 3533 - 3550. doi: 10.1175/JAS-D-20-0008.1

Stevens, B., Satoh, M., Auger, L., Biercamp, J., Bretherton, C. S., Chen, X., ... Zhou, L. (2019). DYAMOND: the DYnamics of the atmospheric general circulation modeled on non-hydrostatic domains. *Progress in Earth and Planetary Science*, *6*(1), 61. doi: 10.1186/s40645-019-0304-z

Straub, K. H., & Kiladis, G. N. (2003). Interactions between the Boreal Summer Intraseasonal Oscillation and Higher-Frequency Tropical Wave Activity. *Mon. Wea. Rev.*, *131*, 945–960. doi: 10.1175/1520-0493(2003)131⟨0945:IBTBSI⟩2.0

.CO;2

Tabari, H. (2020). Climate change impact on flood and extreme precipitation increases with water availability. *Scientific Report*, *10*(1), 13768. doi: 10.1038/s41598-020-70816-2

Takayabu, Y. N., & Nitta, T. (1993). 3-5 day-period disturbances coupled with convection over the tropical pacific ocean. *Journal of the Meteorological Society of Japan. Ser. II*, *71*(2), 221–246. doi: 10.2151/jmsj1965.71.2_221

Taylor, C. M., Belušić, D., Guichard, F., Parker, D. J., Vischel, T., Bock, O., ... Panthou, G. (2017). Frequency of extreme sahelian storms tripled since 1982 in satellite observations. *Nature*, *544*(7651), 475–478. doi: 10.1038/nature22069

Vasconcelos Junior, F. d. C., Jones, C., Gandu, A. W., & Martins, E. S. P. R. (2021). Impacts of the madden-julian oscillation on the intensity and spatial extent of heavy precipitation events in northern northeast brazil. *International Journal of Climatology*, *41*(6), 3628-3639. doi: https://doi.org/10.1002/joc.7039

Vizy, E. K., & Cook, K. H. (2022). Distribution of extreme rainfall events and their environmental controls in the west african sahel and soudan. *Climate Dynamics*, *59*, 997–1026. doi: doi.org/10.1007/s00382-022-06171-x

Wheeler, M., & Kiladis, G. N. (1999). Convectively coupled equatorial waves: Analysis of clouds and temperature in the wavenumber–frequency domain. *J. Atmos. Sci.*, *56*, 374–399. doi: 10.1175/1520-0469(1999)056⟨0374:CCEWAO⟩2.0.CO;2

Wheeler, M. C., & Hendon, H. H. (2004). An all-season real-time multivariate MJO index: Development of an index for monitoring and prediction. *Mon. Wea. Rev.*, *132*, 1917–1932. doi: 10.1175/1520-0493(2004)132⟨1917:AARMMI⟩2.0.CO;2

Wolding, B., Dias, J., Kiladis, G., Maloney, E., & Branson, M. (2020). Interactions between moisture and tropical convection. part ii: The convective coupling of equatorial waves. *Journal of the Atmospheric Sciences*, *77*(5), 1801 - 1819. doi: 10.1175/JAS-D-19-0226.1

Yasunaga, K., & Mapes, B. (2011a). Differences between more divergent and more rotational types of convectively coupled equatorial waves. part II: Composite analysis based on space–time filtering. *Journal of the Atmospheric Sciences*, *69*(1), 17–34. doi: 10.1175/JAS-D-11-034.1

Yasunaga, K., & Mapes, B. (2011b). Differences between more divergent and more rotational types of convectively coupled equatorial waves. part I: Space–time spectral analyses. *Journal of the Atmospheric Sciences*, *69*(1), 3–16. doi: 10.1175/JAS-D-11-033.1

Ying, Y., & Zhang, F. (2017). Practical and intrinsic predictability of multiscale weather and convectively coupled equatorial waves during the active phase of an mjo. *J. Atmos. Sci.*, *74*, 3771–3785.

Zhang, C. (2005). Madden-julian oscillation. *Reviews of Geophysics*, *43*(2), RG2003. doi: 10.1029/2004RG000158

Mesoscale convective systems modulated by convectively coupled equatorial waves

Yuan-Ming Cheng[1], Juliana Dias[1], George Kiladis[1], Zhe Feng[2], L. Ruby Leung[2]

[1]NOAA/Physical Sciences Laboratory, Boulder, Colorado
[2]Atmospheric Sciences and Global Change Division, Pacific Northwest National Laboratory, Richland, Washington

Key Points:

- Mesoscale convective system (MCS) frequency increases during the active phase of convectively coupled equatorial waves (CCEWs).
- MCSs tend to rain harder, produce more lifetime total rain, and grow larger in size when they occur during the active phase of CCEWs.
- The probability of extreme MCSs rises during active CCEWs. This provides an opportunity for extended forecasts of extreme rainfall events.

Corresponding author: Yuan-Ming Cheng, yuan-ming.cheng@noaa.gov

Abstract

Mesoscale convective systems (MCSs) produce over 50% of tropical precipitation and account for the majority of extreme rainfall and flooding events. MCSs are considered the building blocks of larger-scale convectively coupled equatorial waves (CCEWs). While CCEWs can provide favorable environments for convection, how CCEWs can systematically impact organized convection and thereby MCS characteristics is less clear. We examine this question by analyzing a global MCS tracking dataset. During the active phase of CCEWs, MCS frequency increases and MCSs rain harder, produce more lifetime total rain, and grow larger in size. The probability of extreme MCSs also elevates. These changes are most pronounced when MCSs are associated with Kelvin waves and tropical depression-type waves while least so with the Madden-Julian Oscillation. These results can be benchmarks to improve model representation of MCS interactions with large-scale circulations and can be leveraged operationally for extended forecasts of high-impact MCSs.

Plain Language Summary

Satellite observations show that the population of tropical clouds tends to cluster in a variety of sizes. A type of cluster with a size of around 100 km, known as mesoscale convective systems (MCSs), produces over 50% of tropical rainfall and often causes extreme rainfall and flooding events because MCSs can produce heavy rainfall for a long duration. Other larger clusters spanning from 1000 to 10000 km, such as convectively coupled equatorial waves (CCEWs), can favor the formation of convection within them. However, how CCEWs can systematically change MCS development and characteristics is not well understood. We examine this by analyzing an MCS tracking dataset. When MCSs occur within CCEWs, their frequency increases and they rain harder, produce more lifetime total rain, and grow larger in size. The probability of extreme MCSs is also elevated. These changes are most pronounced when MCSs occur within two types of CCEWs, Kelvin waves and tropical depression-type waves while least so with another, the Madden-Julian Oscillation. These results can be benchmarks to improve computer simulations of MCS interactions with large-scale circulations. Because CCEWs are better predicted than MCSs beyond one week, results here can also be leveraged operationally for forecasts of high-impact MCSs.

1 Introduction

Satellite observations of clouds in the tropics reveal a hierarchy of organized cloud clusters ranging from the planetary-scale Madden–Julian Oscillation (MJO), through synoptic-scale convectively coupled equatorial waves (CCEWs), to mesoscale convective systems (MCSs, Nakazawa, 1988; Mapes & Houze, 1993; S. S. Chen et al., 1996). These various types of convective organization are not necessarily independent from one another and MCSs, with scales of 100s of kilometers, are often considered building blocks of those larger-scale tropical circulations (Mapes et al., 2006). The most intense MCSs often cause high-impact weather events and the frequency of these rainfall extremes has increased in the past few decades and is projected to rise with climate change (Z. Feng et al., 2016; Taylor et al., 2017; Tabari, 2020; R. S. Schumacher & Rasmussen, 2020). While MCSs are difficult to predict in current global weather and climate models due to their smaller scales and dependence on subgrid-scale processes, larger-scale disturbances such as CCEWs can be predicted with higher skill beyond one week (Ying & Zhang, 2017; Dias et al., 2018; Janiga et al., 2018; Judt, 2020). Therefore, synoptic disturbances can be useful sources of extended predictability for tropical rainfall events associated with MCSs. A critical step towards this is to establish an observational understanding of how MCS characteristics and their extremes can be related to those large-scale disturbances.

The potential modulation of MCSs by large-scale tropical circulations is somewhat expected considering that 100 years of MCS research invariantly highlights how environmental conditions can impact the initiation, development, and intensity of MCSs over a wide range of climate regimes (e.g., Houze, 2018; Rotunno et al., 1988; LeMone et al., 1998; Laing & Fritsch, 2000). Vertical wind shear can favor convective cells to organize into coherent mesoscale entities. Moisture and entrainment of dry air can impact the ability of convective elements to grow upscale into extensive stratiform regions characteristics of mature MCSs (C. Schumacher & Houze, 2006; X. Chen et al., 2022). The most intense and high-impact MCSs are often a result of interactions across scales generating favorable environments for long-lasting convection (Vizy & Cook, 2022; R. S. Schumacher & Johnson, 2005; Taylor et al., 2017; Latos et al., 2021; Baranowski et al., 2020).

While the term CCEWs is traditionally reserved for convectively coupled Matsuno modes (Matsuno, 1966; Kiladis et al., 2009), here we adopt a broad perspective (Wolding et al., 2020), which also includes the MJO (Madden & Julian, 1971) and tropical depression (TD)-type disturbances or easterly waves (Takayabu & Nitta, 1993; Kiladis et al., 2006). CCEWs can modulate tropical environments to favor convective initiation and organization (Kiladis et al., 2009; Serra et al., 2020). This modulation can impact the ensemble of cloud populations and change the likelihood of MCS occurrence (Mapes et al., 2006; Yasunaga & Mapes, 2011b, 2011a; Nakamura & Takayabu, 2022a, 2022b). In addition, since the structures of CCEWs vary systematically from one another, this influences the ability of different CCEWs to support convection and determines whether groups of convective cells can develop upscale into MCSs. A recently developed 19-year MCS tracking dataset from Z. Feng et al. (2021) offers a unique opportunity to systematically examine the relationship between CCEWs and embedded MCSs across the global tropics.

The goal of this study is to document how MCSs are systematically modulated by CCEWs as part of a broad community effort to further our understanding of convective organization and wave-convection coupling in the tropics. In particular, we address two questions: 1) How do CCEWs modulate MCS frequency, characteristics, and extremes? 2) How does this modulation vary with different CCEWs? This observed relationship between organized convection and large-scale circulations can be benchmarks to improve model representations of MCS interactions with large-scale circulations and provide operational guidance for high-impact MCS events at extended lead times.

2 Data and Method

2.1 CCEW identification

We use the rainfall product of Global Precipitation Mission Integrated Multi-satellitE Retrievals for Global precipitation measurement (GPM IMERG, Huffman et al., 2020) from 2001 to 2019. The IMERG rainfall is utilized at 3-hour intervals and interpolated to 2.5 ° × 2.5 °. To identify CCEWs, tropical rainfall is filtered in wavenumber-frequency space following the standard method from M. Wheeler and Kiladis (1999), with the same parameters as in Dias et al. (2017) for Matsuno's modes and the MJO. For TDs, we apply the same filter as in Kiladis et al. (2006). Due to the large seasonal and regional variation of CCEW activity across the globe (M. Wheeler & Kiladis, 1999; Roundy & Frank, 2004; P. Huang & Huang, 2011; Dias & Kiladis, 2014), amplitudes of the filtered signals are normalized by standard deviation at each grid point using the 3-hourly data with the first three harmonics of seasonal cycle removed. In the interest of conciseness, but still considering seasonal cycles of CCEWs, we present results from March–August for Kelvin waves, June—November for TDs and mixed Rossby gravity waves (MRGs), and November–April for equatorial Rossby waves (ERs) and the MJO. These are the months when each type of CCEWs is most active (not shown).

While we have investigated all CCEWs, we exclude westward and eastward inertio-gravity waves. This is because one underlying assumption is that large-scale circulations provide a relatively unchanged environment within the typical lifetime of MCSs. The lack of scale separation between MCSs and inertio-gravity waves invalidates this assumption.

2.2 MCS database

We use the global MCS database from Z. Feng et al. (2021) where MCSs are tracked hourly from 2001 to 2019 using NASA brightness temperature (T_b) (Janowiak et al., 2017) and precipitation features (PFs) retrieved from the GPM IMERG precipitation product at 0.1° spatial resolution. The two datasets allow for more accurate identification of MCSs where their lifetime evolution and internal structure (such as convective and stratiform features manifested as rain rates) are considered. Briefly, an MCS is identified if the following criteria are met for longer than four hours (see Z. Feng et al. (2021) for more details). 1) A cold cloud system defined in T_b exceeds an area of 4×10^4 km^2 and contains at least a PF in IMERG with a major axis length larger than 100 km. 2) The PF area, mean rain rate, rain rate skewness, and heavy rain volume ratio are larger than corresponding lifetime-dependent thresholds. MCSs in the tropics are tracked in two domains and stitched together. The two domains are combined by allowing MCSs to track from east to west but not in the opposite direction near the boundaries (30°–50°E and 180°). As a result, MCS tracks in those regions need to be interpreted with caution. Only MCSs within 15°N/S are analyzed.

2.3 MCS characteristics

In the MCS dataset, each cold cloud system has hourly centroid latitudes and longitudes. These values are averaged across the MCS lifetime to obtain a mean location and time of that MCS. If the corresponding amplitude of a CCEW, measured by the nearest grid points to the mean MCS location and the closest 3-hourly time stamp to the average MCS time, is equal to or larger than one standard deviation, the MCS is determined to be concurrent with that active CCEW. Note that since tropical convection is organized at various time scales, an MCS can be associated with more than one type of active CCEWs.

We calculate five representative characteristics of MCSs to assess their intensity, sizes, and duration. The three intensity metrics are lifetime total rain, average rain rate, and maximum rain rate. The lifetime total rain is the integrated amount of rain, expressed in millimeters (mm), falling underneath an MCS cloud shield throughout its lifetime. This metric can be converted to volumetric rain in kilograms. The average rain rate, measured in mm hr^{-1}, is the mean rain rate of the largest 3 PFs of an MCS throughout its lifetime. Three PFs are used because the MCS tracking dataset only includes precipitation statistics from the largest 3 PFs, which on average produce over 70% of the lifetime total precipitation. The maximum rain rate, expressed in mm hr^{-1}, is defined as the heaviest precipitating pixel within the cloud shield during the lifetime of an MCS. The size of an MCS is expressed in km^2 as the mean area of the cold cloud shield during its lifetime. The duration is the total hours of each tracked cold cloud system. Every MCS has one value for each of these metrics to represent its overall characteristics.

We bin MCSs into 5° × 5° grid boxes. Values of MCS characteristics are standardized by the mean and standard deviation of all MCSs occurring in the same grid box and months. Despite tremendous MCS variability globally and seasonally (Houze et al., 2015; X. Huang et al., 2018; Schiro et al., 2020; Z. Feng et al., 2021), using this dimensionless Z-score in probability distribution functions (pdfs) renders distributions of MCS characteristics similar across the globe (not shown). The choice of grid-box sizes is made because the area of an individual MCS is at least 2° × 2° and this binning yields robust

statistical analysis. Tests reveal that the size of the grids does not qualitatively impact the results.

2.4 MCS frequency and risk ratio for extreme MCSs

Two ratios are defined to assess the change in MCS frequency attributable to CCEWs relative to the climatology. A frequency ratio for MCS occurrence R_{freq} in each grid box is defined as,

$$R_{freq} = \frac{\mathrm{MCS}_{wave}/\mathrm{t}_{wave}}{\mathrm{MCS}_{all}/\mathrm{t}_{all}} \tag{1}$$

MCS_{wave} is the number of MCSs concurrent with a particular CCEW, and t_{wave} is the number of times when that CCEW is active. MCS_{all} is the total number of MCSs, and t_{all} is the total number of times. For each CCEW type, all numbers are calculated for the respective 6-month periods considered from 2001 to 2019. The numerator of R_{freq} describes the frequency of MCSs when that CCEW is active and the denominator is the climatological frequency of MCSs. Taken together, R_{freq} measures the MCS frequency change associated with that CCEW normalized by climatology. A value larger than one indicates the presence of the CCEW increases the frequency of MCSs.

Similarly, we define a risk ratio to measure the frequency change of extreme MCSs. The threshold for extreme MCSs is defined as the top 10 percentile at each grid box for each 6-month period, so the climatological probability of an extreme MCS is 10%. The extremes are calculated for each of the five MCS characteristics. We define the risk ratio R_{risk} at each location as,

$$R_{risk} = \frac{\text{Extreme } \mathrm{MCS}_{wave}/\mathrm{MCS}_{wave}}{10\%}. \tag{2}$$

Extreme MCS_{wave} denotes the number of extreme MCSs concurrent with a particular CCEW. "Extreme MCS_{wave}" is normalized by the counts of MCSs concurrent with the CCEW because different waves modulate the MCS occurrence differently. The numerator as a whole calculates the probability of an MCS being categorized as extreme out of all the MCSs associated with that particular CCEW. A value of R_{risk} larger than one shows that the CCEW elevates the probability of extreme MCSs relative to a climatological value of 10%.

3 Climatological and CCEW-modulated MCS frequency

The distribution of MCS occurrence (colors in Fig. 1a) closely follows the mean tropical precipitation (contours). The frequency of MCSs is highest along the Intertropical Convergence Zone (ITCZ) where the annual precipitation is high. This correspondence between MCS counts and rainfall holds true for different seasons such that the MCS counts closely follow the migration of the ITCZ (Fig. S1). Nonetheless, the MCS occurrence does not solely depend on the mean precipitation. Landmasses, regardless of continents or islands, accumulate the highest counts of MCSs, although these regions generally show less annual rainfall than the adjacent ocean. Given that the percentage of MCS rainfall remains similar at 50–70% across the tropics (Fig 10 of Z. Feng et al., 2021), the high number of MCSs over land suggests that they produce less lifetime total rain than the oceanic ones (see also Fig. S3). Over the ocean, MCSs are most frequent over the warm pool and South Pacific Convergence Zone, as well as along the ITCZ in the Western Hemisphere. This global distribution is consistent with studies using various tracking algorithms on different satellite products (Houze et al., 2015; X. Huang et al., 2018) and reaffirms the validity of the MCS database.

Figure 1b-1d shows an increase in the MCS frequency associated with active CCEWs, as indicated by R_{freq} larger than 1 (red shading). This increase in frequency is consistent with the interpretation that convective envelopes of CCEWs favor upscale growth

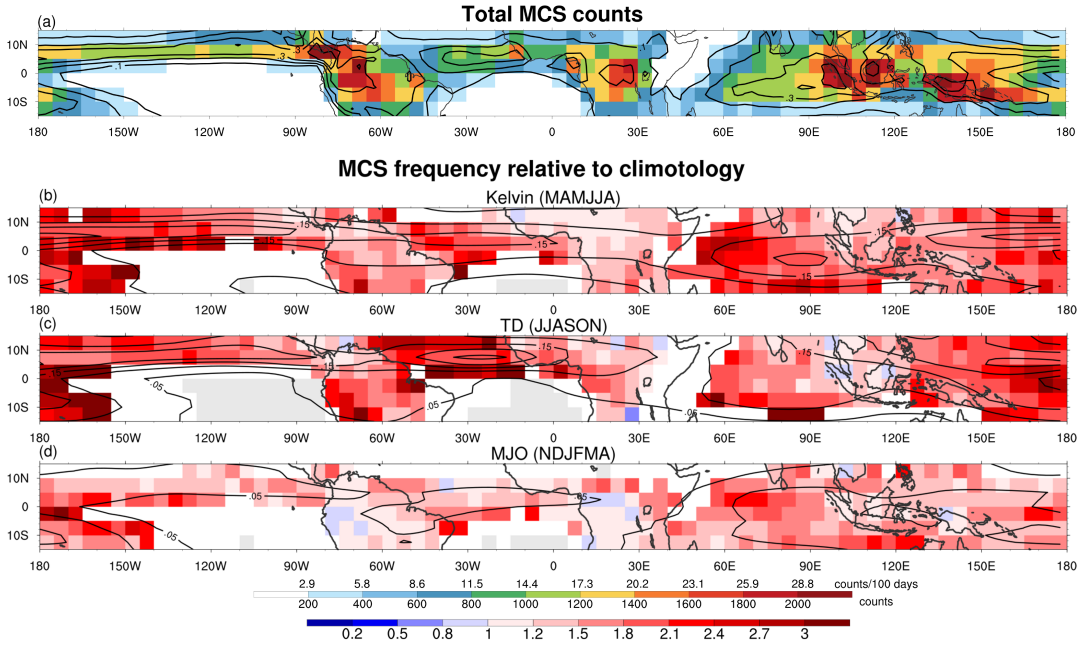

Figure 1. (a) MCS counts binned in 5° × 5° grid boxes from 2001 to 2019. Each MCS is binned by its average lifetime location. Annual mean precipitation is contoured at 0.1 mm hr^{-1}. (b)-(d) Frequency ratio (R_{freq}, colors) of MCS occurrence relative to climatology when the calculation is conditioned on (b) Kelvin waves in MAMJJA, (c) TDs in JJASON, and (d) the MJO in NDJFMA. The mean standard deviation of wave-filtered rainfall in the respective months is contoured every 0.05 mm hr^{-1} with zero lines omitted.

of convection, support the development of MCS, and thereby increase the MCS frequency. This modulation is stronger over the ocean for all CCEWs (also Fig. S2). The average R_{freq} for Kelvin waves, TDs, and the MJO over the ocean is 2.0, 2.2, and 1.6 compared to 1.4, 1.5, and 1.3 over the land. The lack of other forcing mechanisms over the ocean, such as the diurnal cycle and topography (Sakaeda et al., 2020), likely renders CCEWs more effective in supporting MCSs than over land.

The darker red shadings of R_{freq} for Kelvin waves and TDs compared to the MJO (Fig. 1b-1d) indicate stronger modulation by the former two. In fact, Kelvin waves and TDs are the two most effective modulators, followed by MRGs and ERs, and trailed by the MJO (Fig. S2). While numerous studies have highlighted the MJO as an important modulator of tropical rainfall and extreme events (e.g., Jones et al., 2004; Grimm, 2019; Schreck III, 2021; Vasconcelos Junior et al., 2021), these results suggest that synoptic-scale CCEWs influence convective organization and precipitation even more strongly than the MJO (Fink & Reiner, 2003; Linden et al., 2016; Schlueter et al., 2018; Ferrett et al., 2020; Latos et al., 2021; Lubis et al., 2022).

The elevated MCS frequency (shading in Fig. 1b-1d) overall matches well with climatological CCEW activity (contours). Kelvin waves modulate MCS frequency most strongly over the Indo-Pacific warm pool and the east Pacific but less so from South America to

Africa, consistent with the activity of Kelvin waves (Roundy & Frank, 2004; P. Huang & Huang, 2011). On the contrary, TD frequency modulation is stronger over Africa and the Atlantic, as well as the Pacific. These regions are known for strong easterly wave activity during northern summer and fall (Kiladis et al., 2006; Rydbeck & Maloney, 2014; Cheng et al., 2019; T. Feng et al., 2020). Lastly, the modulation by the MJO appears stronger over the Eastern than Western Hemisphere, consistent with the MJO's strong precipitation and circulations over the warm pool (M. C. Wheeler & Hendon, 2004; Zhang, 2005). Note that wavenumber-frequency filtering cannot unambiguously identify CCEWs (Sakaeda et al., 2020; Cheng et al., 2022; Knippertz et al., 2022), so R_{freq} in regions with climatologically low wave activity should be interpreted with caution.

4 MCS characteristics and their changes associated with CCEWs

Figure 2 shows the covariability of MCS characteristics in joint pdfs. The pdf estimates are calculated by binning MCS characteristics according to their Z-scores (Sec. 2.3). In this standardized format, zeros mark the mean at each grid box and the nonzero integers indicate the number of standard deviations from the mean. To aid interpretation, physical quantities corresponding to the Z-scores in various regions are provided in Fig. S3. In all panels of Fig. 2, we choose lifetime total rain as a benchmark variable in all y-axes because 1) it is an integrated measure of MCS's socioeconomic impact as it is a function of rain rates, sizes, and duration, and 2) it is a representative metric for approximating latent heat release important for wave–convection coupling (Nakamura & Takayabu, 2022a; Chien & Kim, 2023; Rios-Berrios et al., 2023). The x-axis denotes four other MCS characteristics in each column: average rain rates, maximum rain rates, sizes, and duration (defined in Sec. 2.3).

The climatological pdfs (Fig.2a–2d) demonstrate the diverse behaviors of MCSs. For instance, MCSs with a high amount of lifetime total rain at 2 standard deviations above the mean is comprised of those with average and maximum rain rates ranging from -1 to 4 standard deviations, as well as sizes and duration from -1 to 5. The median of lifetime total rain for each bin in both intensity metrics (black dots in Fig. 2a and 2b) levels off for rain rates above 2 standard deviations. Indeed, both intensity metrics are only moderately correlated with lifetime total rain (correlation coefficients of 0.35 and 0.48). This suggests that heavy rain rates alone do not necessarily produce a high amount of lifetime total rain because heavy rain may not be sustained for a long time or cover a large area. On the contrary, lifetime total rain is strongly correlated with sizes and duration (0.72 and 0.69, Fig. 2c and 2d). This indicates that MCSs covering a large area and/or lasting for a long period of time are very likely to produce high amounts of lifetime total rain. It is worth noting that sizes and duration are only weakly correlated at 0.28 (not shown), suggesting that a large MCS is not necessarily long-lived and vice versa.

The pdfs of MCS characteristics change substantially when MCSs are conditioned on active CCEWs (bottom three rows of Fig. 2). In the first three panels for Kelvin waves (Fig. 2e–2g), the population decreases (blue shading) in the low-left corner and increases in the upper-right (red shading). This change indicates that MCSs rain harder, produce more lifetime total rain, and grow larger in size when they are concurrent with active Kelvin waves. For duration vs. lifetime total rain (Fig. 2h), the population shifts toward the upper-left corner, which suggests two related interpretations. 1) For a given duration of MCSs, those collocated with active Kelvin waves produce more rain (green vs. black dots). 2) For a given amount of lifetime total rain, the MCS duration tends to be shorter. This population change indicates that the MCSs are more "efficient" in producing the same amount of lifetime total rain, suggesting an increase in rain rates and/or sizes, consistent with Fig. 2e–2g.

Nearly identical shifts of MCS characteristics occur when TDs are active (2i–2l). For the MJO, a similar pattern change is observed but the amplitude is weaker than Kelvin

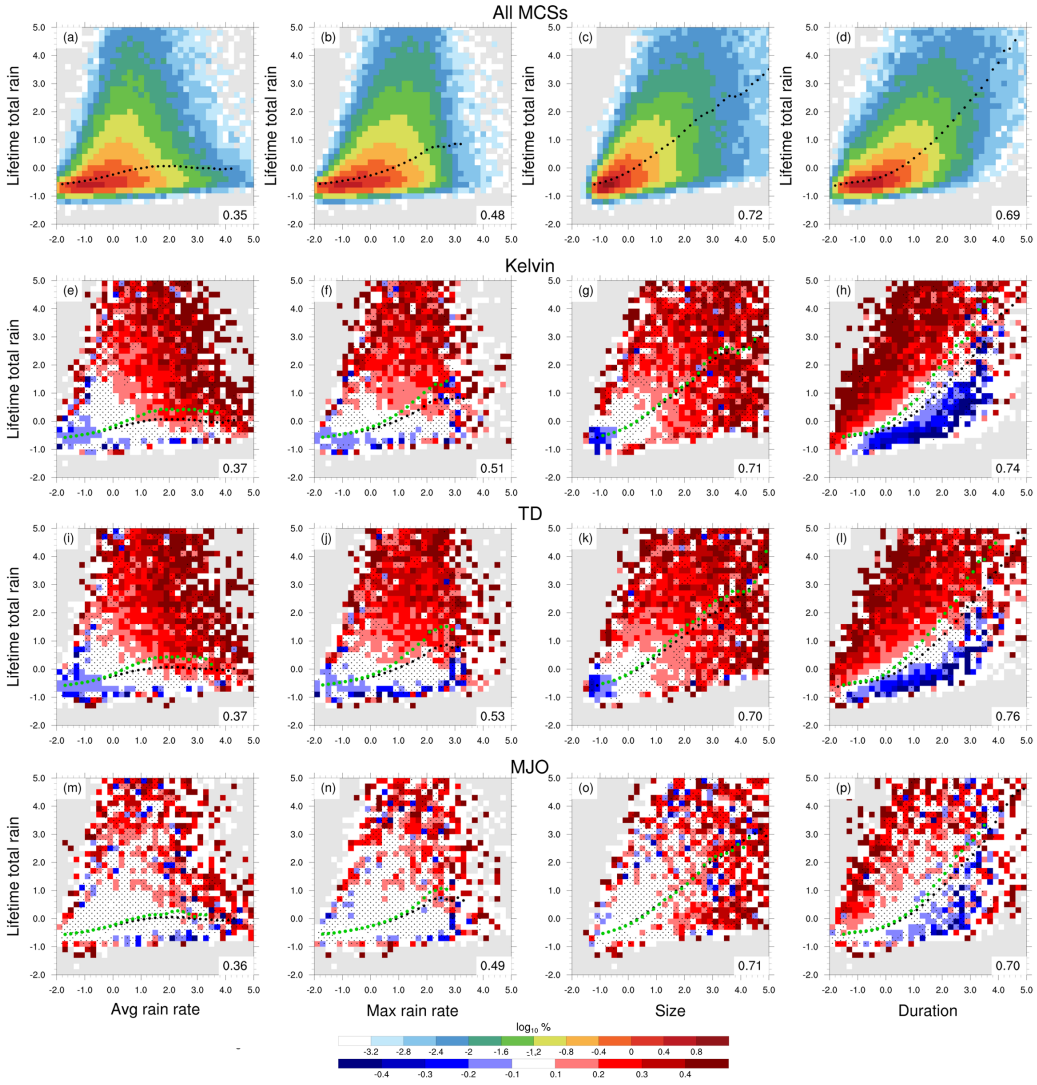

Figure 2. Top row (a–d): Joint probability distribution functions (pdfs) of MCS characteristics for all MCSs. Bottom three rows: Change of pdfs from all-MCS ones when MCSs are conditioned on (e–h) Kelvin waves, (i–l) TDs, and (m–p) the MJO. The first column shows pdfs for average rain rate vs. lifetime total rain; the second maximum rain rate vs. lifetime total rain; the third sizes vs. lifetime total rain; the fourth duration vs. lifetime total rain. In the first row, color shadings indicate the log_{10} of the percentage of total MCS counts in each bin while in the bottom three rows, colors show the log_{10} percentage change from all-MCS pdfs. Numbers on the lower-right corner of each panel denote the correlation coefficient between the two variables for all MCSs (top row) and those conditioned on CCEWs (bottom three rows). Black dots denote the median of lifetime total rain binned by the four characteristics in the x-axis for all MCSs and green dots mark the same median but for CCEW-conditioned MCSs. Stippling shows bins that are statistically *not* significant from the all-MCS pdf at the 95% interval estimated using 1000 times random sampling. Gray shading indicates bins with no MCS occurrence.

waves and TDs. Indeed, similar pattern changes occur for all CCEWs, but the amplitude of modulation differs (Fig. S4). Kelvin waves and TDs exhibit the most pronounced change in characteristics, followed by MRGs and ERs, trailed by the MJO. These systematic changes confirm that all CCEWs provide environments for MCSs to rain harder, produce more rain, and grow larger in size, although the extent of these enhancements depends on the type of CCEWs.

A natural question related to the change of characteristics is: do MCSs concurrent with active CCEWs behave differently from those without? Interestingly, the correlation among MCS characteristics, conditioned on CCEWs or not, remains remarkably similar, as shown by the correlation coefficients on the lower right corner of each panel in Figs. 2 and S4. This suggests that the change does not favor one characteristic over the other. Instead, the convective envelope of CCEWs provides a favorable environment for MCS development, but the underlying MCS dynamics likely remain similar with or without CCEWs.

5 Risks of extreme MCSs associated with CCEWs

The fact that MCSs tend to rain harder, produce more lifetime total rain, and develop into larger systems when they occur within active large-scale circulations suggests a more frequent occurrence of extreme MCSs associated with CCEWs. In this section, we investigate extreme MCSs with respect to the five characteristics used so far. Using all five metrics is because a single one cannot thoroughly depict the range of socioeconomic impacts of extreme rainfall events. For instance, extremely heavy rain rates can cause severe local flash floods while an extremely high amount of lifetime total rain can lead to widespread flooding.

The risk ratio R_{risk} measures the frequency change of extreme MCSs due to CCEWs (Sec. 2.4). Recall that a value of R_{risk} larger than one indicates that CCEWs elevate the probability of extreme MCSs relative to the climatological value of 10%. Figures 3a-3c and S5 show that CCEWs generally elevate the probability of MCSs with extremely high amounts of lifetime total rain (red colors). Kelvin waves and TDs elevate the risk by a factor of two across the majority of the tropics. Interestingly, tropical Africa shows mixed signals by Kelvin waves but a strong increase by TDs. Kelvin waves are known to modulate precipitation (Nguyen & Duvel, 2008; Mekonnen & Thorncroft, 2016; Schlueter et al., 2018, 2019) and extreme rainfall (Lafore et al., 2017; Nicholson et al., 2022) over Africa. However, Fig. 3b shows that TDs, or African easterly waves, are more strongly correlated with extreme MCS rainfall events, consistent with Vizy and Cook (2022). The MJO shows overall slight increases in probability but those increases are interspersed with decreases around the globe (Fig. 3c). The most robust increase appears over the Indian Ocean and the equatorial Maritime Continent, consistent with strong MJO signals in the region and previous studies (M. C. Wheeler & Hendon, 2004; Zhang, 2005; Da Silva & Matthews, 2021; Schreck III, 2021; Lubis et al., 2022). The mixed probability over South America and Africa is somewhat similar to the noisy signal in Schreck III (2021) but slightly at odds with Vasconcelos Junior et al. (2021) over South America, likely due to a different definition of extreme events. R_{risk} for MCSs with extreme maximum rain rates shows a remarkably similar pattern (Fig S6) to Fig. 3a–3c.

Figure 3d summarizes the global average of statistically significant R_{risk} for each of the characteristics. Kelvin waves and TDs nearly double the probabilities of extreme MCSs in all MCS characteristics (lifetime total in red, two rain intensity metrics in orange and yellow, and sizes in green) except for duration (blue). Interestingly, for both types of CCEWs, while there is slight variation in the amplitude of modulation (R_{risk} ranging from 1.7 to 1.9), the prevalence of extreme MCSs, as measured by the percentage of the global tropics showing statistically significant signals, differentiates the modulation of one characteristic from another. More than 60% of the tropics shows more fre-

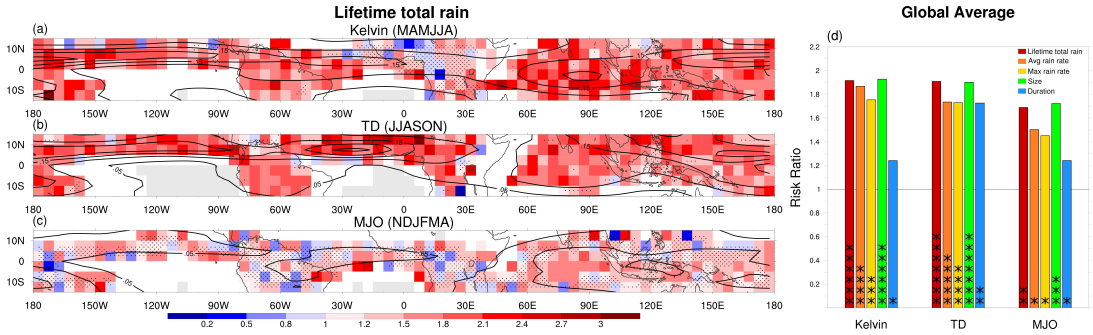

Figure 3. Risk ratio (R_{risk}) for MCSs with extremely high lifetime total rain for (a) Kelvin waves, (b) TDs, and (c) the MJO. Mean standard deviation of wave-filtered rainfall in the respective 6 months is contoured every 0.05 mm hr^{-1}. (d) Average R_{risk} for CCEWs over the global tropics where the risk ratio is statistically significant at the 95% interval. Asterisks indicate how prevalent statistically significant signals are. Each asterisk represents 10% of the grid boxes in the global tropics. In (a)–(c), stippling marks statistically *not* significant regions at the 95% interval estimated using 1000 times random sampling. Grid boxes accumulating less than 100 counts of MCSs over the 6 months during 2001–2019 are plotted white and those with no MCS occurrence gray. In (d), the legend shows different flavors of extreme MCSs in various colors.

quent extremely large MCSs and extremely high lifetime total rain, compared to only 30–50% of the tropics having extremely heavy rain rates. Similarly, the MJO elevates R_{risk} for the lifetime total rain, intensity, and sizes but to a weaker extent (R_{risk} ranging from 1.4 to 1.7) and over fewer regions (10–30% of the global tropics). The relationship between CCEWs and extreme MCSs, as measured by R_{risk} and its prevalence, is strongest for Kelvin waves and TDs, followed by MRGs and ERs, and trailed by the MJO (Fig S5, S6, and S7).

CCEWs marginally modulate the probability of extremely long-lasting systems. The R_{risk} (blue) is increased to 1.7 by TDs and to 1.2 by Kelvin waves and the MJO. Nonetheless, the areas affected by all types of CCEWs are limited to 10–20% of the tropics, much lower than other MCS characteristics. This weak modulation of extremely long-lived MCSs is consistent with the marginal impact of CCEWs on MCS duration (not shown).

6 Conclusions and Discussions

Our analysis of MCSs using satellite-derived tropical cloudiness and rainfall demonstrates that MCSs are modulated by CCEWs. More specifically, when MCSs are concurrent with active CCEWs: 1) MCSs occur more frequently (Fig. 1). 2) MCSs tend to rain harder, produce more lifetime total rain, and grow larger in size (Fig. 2). 3) The probability of extreme MCSs is elevated across a large portion of the tropics (Fig. 3). 4) These changes in MCS frequencies and characteristics are most pronounced when MCSs are associated with Kevin waves and TDs, followed by the MRGs and ERs, and trailed by the MJO.

We have also found that different MCS characteristics are modulated by CCEWs to varying degrees. While mesoscale clustering generally enhances tropical precipitation (Angulo-Umana & Kim, 2023), the interplay among physical constraints, such as moisture sources from moisture convergence and surface fluxes (Doswell et al., 1996), the energetics of ocean-atmosphere discharge-recharge cycles (S. S. Chen et al., 2016), and the extent of favorable MCS environments provided by CCEWs likely determines the am-

plitude of enhancements. Interestingly, while CCEWs may favor mesoscale convective organization, the fact that correlations among MCS characteristics are relatively insensitive to CCEWs (Fig. 2) indicates that CCEWs do not fundamentally alter MCS dynamics.

The varying strengths of MCS modulation among CCEWs are likely rooted in their differing convective coupling mechanisms (Yasunaga & Mapes, 2011b; Wolding et al., 2020; Nakamura & Takayabu, 2022b; Adames, 2022; Sakaeda & Torri, 2022). CCEWs such as the MJO and ER are primarily driven by moisture variability. Others such as Kelvin waves and African easterly waves demonstrate strong gravity wave characteristics where adiabatic motions driven by wave dynamics play a key role in convective coupling. In addition, the different convective evolution observed in Kelvin waves and ERs suggests that the stretched building block hypothesis may not explain convective coupling across all CCEWs (Nakamura & Takayabu, 2022b). These differing coupling mechanisms warrant further investigation to better understand the interactions between convective and large-scale circulations (Houze et al., 2000; Ocasio et al., 2020).

We note the following caveats of this study. Convective organization occurs across time scales (Gottschalck et al., 2013; Peatman et al., 2021) and wavenumber-frequency filtering cannot unambiguously identify CCEWs (Sakaeda et al., 2020; Cheng et al., 2022; Knippertz et al., 2022). One may argue that the stronger modulation from higher-frequency CCEWs can be attributed to MCS projection onto the wavenumber-frequency space due to comparable spatial and temporal scales. However, we have found that the amplitude of the waves is weakly correlated with MCS characteristics (not shown), suggesting that other physical mechanisms contribute to the MCS-CCEW relationship. A related caveat is the weaker modulation by the MJO. This could be the result of interference among enhanced and suppressed phases of smaller-scale CCEWs embedded in the MJO planetary-scale convective envelope (Straub & Kiladis, 2003; Roundy, 2008; Dias et al., 2013, 2017).

Our results have the following potential implications. From a model development perspective, organized convection has been poorly represented in global models with convection parameterization (Moncrieff et al., 2017) and marginally constrained in cloud-permitting models (Stevens et al., 2019). Various characteristics used here such as size and duration in observations can be utilized as benchmarks for model development. Studies have also shown that either incorporating the aggregated effects of organized convection in cumulus parameterization (Moncrieff et al., 2017; Bengtsson et al., 2021) or using cloud-resolving capabilities (Judt & Rios-Berrios, 2021; Rios-Berrios et al., 2023; Jung & Knippertz, 2023) can improve model representation of CCEWs. However, whether these models can reproduce MCS modulations by the large-scale forcing documented here needs to be investigated. In addition, the results regarding extreme MCSs suggest that forecasts of high-impact events at long lead times need to consider forecasts of CCEWs along with those of the MJO. This statistical analysis may be combined with global models to provide a probabilistic forecast of extremes at extended lead times.

Acknowledgments

YMC is grateful for the National Research Council postdoctoral research associateship at NOAA Physical Sciences Laboratory. ZF and LRL are supported by the Office of Science, U.S. Department of Energy Biological and Environmental Research as part of the Regional and Global Model Analysis program area. Pacific Northwest National Laboratory is operated for the Department of Energy by Battelle Memorial Institute under contract no. DE-AC05-76RL01830. We also thank Brandon Wolding and Stefan Tulich whose contributions helped improve the analysis and discussion.

Data Availability Statement

The GPM IMERG precipitation data can be accessed from NASA Goddard Earth Sciences Data and Information Services Center at https://doi.org/10.5067/GPM/IMERG/3B-HH/06. The global Merged IR data can be obtained from NASA Goddard Earth Sciences Data and Information Services Center at https://doi.org/10.5067/P4HZB9N27EKU. The MCS tracking algorithm is open source and detailed in Z. Feng et al. (2022).

References

Adames, A. F. (2022). The basic equations Under Weak temperature gradient balance: Formulation, scaling, and types of convectively-coupled motions. *Journal of the Atmospheric Sciences*, *-1*. doi: 10.1175/JAS-D-21-0215.1

Angulo-Umana, P., & Kim, D. (2023). Mesoscale convective clustering enhances tropical precipitation. *Science Advances*, *9*(2), eabo5317. doi: 10.1126/sciadv.abo5317

Baranowski, D. B., Flatau, M. K., Flatau, P. J., Karnawati, D., Barabasz, K., Labuz, M., ... Marzuki (2020). Social-media and newspaper reports reveal large-scale meteorological drivers of floods on Sumatra. *Nat Commun*, *11*, 2503. doi: doi.org/10.1038/s41467-020-16171-2

Bengtsson, L., Dias, J., Tulich, S., Gehne, M., & Bao, J.-W. (2021). A stochastic parameterization of organized tropical convection using cellular automata for global forecasts in NOAA's unified forecast system. *Journal of Advances in Modeling Earth Systems*, *13*(1), e2020MS002260. doi: 10.1029/2020MS002260

Chen, S. S., Houze, R. A., & Mapes, B. E. (1996). Multiscale variability of deep convection in relation to large-scale circulation in TOGA COARE. *Journal of the Atmospheric Sciences*, *53*(10), 1380–1409. doi: 10.1175/1520-0469(1996)053⟨1380:MVODCI⟩2.0.CO;2

Chen, S. S., Kerns, B. W., Guy, N., Jorgensen, D. P., Delanoë, J., Viltard, N., ... Savarin, A. (2016). Aircraft observations of dry air, the ITCZ, convective cloud systems, and cold pools in MJO during DYNAMO. *Bulletin of the American Meteorological Society*, *97*(3), 405–423. doi: 10.1175/BAMS-D-13-00196.1

Chen, X., Leung, L. R., Feng, Z., & Yang, Q. (2022). Precipitation-moisture coupling over tropical oceans: Sequential roles of shallow, deep, and mesoscale convective systems. *Geophysical Research Letters*, *49*(7), e2022GL097836. doi: 10.1029/2022GL097836

Cheng, Y.-M., Thorncroft, C. D., & Kiladis, G. N. (2019). Two Contrasting African Easterly Wave Behaviors. *J. Atmos. Sci.*, *76*, 1753–1768. doi: 10.1175/JAS-D-18-0300.1

Cheng, Y.-M., Tulich, S., Kiladis, G. N., & Dias, J. (2022). Two extratropical pathways to forcing tropical convective disturbances. *Journal of Climate*, *35*(20), 2987–3009. doi: 10.1175/JCLI-D-22-0171.1

Chien, M.-T., & Kim, D. (2023). Representation of the convectively coupled kelvin waves in modern reanalysis products. *Journal of the Atmospheric Sciences*, *80*(2), 397–418. Retrieved from `https://journals.ametsoc.org/view/journals/atsc/80/2/JAS-D-22-0067.1.xml` doi: 10.1175/JAS-D-22-0067.1

Da Silva, N. A., & Matthews, A. J. (2021). Impact of the madden–julian oscillation on extreme precipitation over the western maritime continent and southeast asia. *Quarterly Journal of the Royal Meteorological Society*, *147*(739), 3434-3453. doi: doi.org/10.1002/qj.4136

Dias, J., Gehne, M., Kiladis, G. N., Sakaeda, N., Bechtold, P., & Haiden, T. (2018). Equatorial waves and the skill of ncep and ecmwf numerical weather prediction systems. *Mon. Wea. Rev.*, *146*, 1763 - 1784. doi: 10.1175/MWR-D-17-0362.1

Dias, J., & Kiladis, G. N. (2014). Influence of the basic state zonal flow on convectively coupled equatorial waves. *Geophysical Research Letters*, 6904–6913. doi: 10.1002/2014GL061476

Dias, J., Leroux, S., Tulich, S. N., & Kiladis, G. N. (2013). How systematic is organized tropical convection within the MJO? *Geophysical Research Letters*, *40*. doi: 10.1002/grl.50308

Dias, J., Sakaeda, N., Kiladis, G. N., & Kikuchi, K. (2017). Influences of the MJO on the space-time organization of tropical convection. *Journal of Geophysical Research: Atmospheres*, *122*(15), 8012-8032. doi: doi.org/10.1002/2017JD026526

Doswell, C. A., Brooks, H. E., & Maddox, R. A. (1996). Flash flood forecasting: An ingredients-based methodology. *Weather and Forecasting*, *11*(4), 560–581. doi: 10.1175/1520-0434(1996)011⟨0560:FFFAIB⟩2.0.CO;2

Feng, T., Yang, X.-Q., Yu, J.-Y., & Huang, R. (2020). Convective coupling in tropical-depression-type waves. part i: Rainfall characteristics and moisture structure. *Journal of the Atmospheric Sciences*, *77*(10), 3407–3422. doi: 10.1175/JAS-D-19-0172.1

Feng, Z., Hardin, J., Barnes, H. C., Li, J., Leung, L. R., Varble, A., & Zhang, Z. (2022). PyFLEXTRKR: a flexible feature tracking python software for convective cloud analysis. *EGUsphere*, 1–29. doi: 10.5194/egusphere-2022-1136

Feng, Z., Leung, L. R., Hagos, S., Houze, R. A., Burleyson, C. D., & Balaguru, K. (2016, November). More frequent intense and long-lived storms dominate the springtime trend in central US rainfall. *Nature Communications*, *7*(1), 13429. doi: 10.1038/ncomms13429

Feng, Z., Leung, L. R., Liu, N., Wang, J., Houze Jr, R. A., Li, J., ... Guo, J. (2021). A global high-resolution mesoscale convective system database using satellite-derived cloud tops, surface precipitation, and tracking. *Journal of Geophysical Research: Atmospheres*, *126*(8), e2020JD034202. doi: doi.org/10.1029/2020JD034202

Ferrett, S., Yang, G.-Y., Woolnough, S. J., Methven, J., Hodges, K., & Holloway, C. E. (2020). Linking extreme precipitation in southeast asia to equatorial waves. *Quarterly Journal of the Royal Meteorological Society*, *146*(727), 665-684. doi: https://doi.org/10.1002/qj.3699

Fink, A. H., & Reiner, A. (2003). Spatiotemporal variability of the relation between African easterly waves and west African squall lines in 1998 and 1999. *J. Geophys. Res.*, *108*, 4332. doi: 10.1029/2002JD002816

Gottschalck, J., Roundy, P. E., Iii, C. J. S., Vintzileos, A., & Zhang, C. (2013). Large-scale atmospheric and oceanic conditions during the 2011–12 DYNAMO field campaign. *Monthly Weather Review*, *141*(12), 4173–4196. Retrieved from `https://journals.ametsoc.org/view/journals/mwre/141/12/mwr-d-13-00022.1.xml` doi: 10.1175/MWR-D-13-00022.1

Grimm, A. M. (2019). Madden–julian oscillation impacts on south american summer monsoon season: precipitation anomalies, extreme events, teleconnections, and role in the MJO cycle. *Clim Dyn*, *53*(1), 907–932. doi: 10.1007/s00382-019-04622-6

Houze, R. A. (2018). 100 years of research on mesoscale convective systems. *Meteorological Monographs*, *59*, 17.1 - 17.54. doi: 10.1175/AMSMONOGRAPHS-D-18-0001.1

Houze, R. A., Chen, S. S., Kingsmill, D. E., Serra, Y., & Yuter, S. E. (2000). Convection over the pacific warm pool in relation to the atmospheric kelvin-rossby wave. *Journal of the Atmospheric Sciences*, *57*(18), 3058–3089. doi: 10.1175/1520-0469(2000)057⟨3058:COTPWP⟩2.0.CO;2

Houze, R. A., Rasmussen, K. L., Zuluaga, M. D., & Brodzik, S. R. (2015). The variable nature of convection in the tropics and subtropics: A legacy of 16 years of the tropical rainfall measuring mission satellite. *Reviews of Geophysics*, *53*(3), 994-1021. doi: https://doi.org/10.1002/2015RG000488

Huang, P., & Huang, R. (2011). Climatology and interannual variability of convectively coupled equatorial waves activity. *J. Climate*, *24*(16), 4451–4465. doi:

10.1175/2011JCLI4021.1

Huang, X., Hu, C., Huang, X., Chu, Y., Tseng, Y.-h., Zhang, G. J., & Lin, Y. (2018). A long-term tropical mesoscale convective systems dataset based on a novel objective automatic tracking algorithm. *Climate Dynamics*, *51*(7), 3145–3159. doi: 10.1007/s00382-018-4071-0

Huffman, G. J., Bolvin, D. T., Braithwaite, D., Hsu, K.-L., Joyce, R. J., Kidd, C., ... Xie, P. (2020). Integrated multi-satellite retrievals for the global precipitation measurement GPM mission IMERG. In V. Levizzani, C. Kidd, D. B. Kirschbaum, C. D. Kummerow, K. Nakamura, & F. J. Turk (Eds.), *Satellite precipitation measurement: Volume 1* (pp. 343–353). Cham: Springer International Publishing. doi: 10.1007/978-3-030-24568-9_19

Janiga, M. A., Schreck, C. J., Ridout, J. A., Flatau, M., Barton, N. P., Metzger, E. J., & Reynolds, C. A. (2018). Subseasonal forecasts of convectively coupled equatorial waves and the mjo: Activity and predictive skill. *Mon. Wea. Rev.*, *146*. doi: 10.1175/MWR-D-17-0261.1

Janowiak, J., Joyce, B., & Xie, P. (2017). Ncep/cpc l3 half hourly 4km global (60s - 60n) merged ir V1 [dataset]. *Goddard Earth Sciences Data and Information Services Center (GES DISC)*. doi: 10.5067/P4HZB9N27EKU

Jones, C., Waliser, D. E., Lau, K. M., & Stern, W. (2004). Global occurrences of extreme precipitation and the madden–julian oscillation: Observations and predictability. *Journal of Climate*, *17*(23), 4575–4589. doi: 10.1175/3238.1

Judt, F. (2020). Atmospheric predictability of the tropics, middle latitudes, and polar regions explored through global storm-resolving simulations. *J. Atmos. Sci.*, *77*, 257 - 276. doi: 10.1175/JAS-D-19-0116.1

Judt, F., & Rios-Berrios, R. (2021). Resolved convection improves the representation of equatorial waves and tropical rainfall variability in a global nonhydrostatic model. *Geophysical Research Letters*, *48*(14), e2021GL093265. doi: 10.1029/2021GL093265

Jung, H., & Knippertz, P. (2023). Link between the time-space behavior of rainfall and 3d dynamical structures of equatorial waves in global convection-permitting simulations. *Geophysical Research Letters*, *50*(2), e2022GL100973. doi: 10.1029/2022GL100973

Kiladis, G. N., Thorncroft, C. D., & Hall, N. M. J. (2006). Three-Dimensional Structure and Dynamics of African Easterly Waves. Part I: Observations. *J. Atmos. Sci.*, *63*, 2212–2230. doi: 10.1175/JAS3741.1

Kiladis, G. N., Wheeler, M. C., Haertel, P. T., Straub, K. H., & Roundy, P. E. (2009). Convectively coupled equatorial waves. *Rev. Geophys.*, *47*, RG2003. doi: 10.1029/2008RG000266

Knippertz, P., Gehne, M., Kiladis, G. N., Kikuchi, K., Rasheeda Satheesh, A., Roundy, P. E., ... Wheeler, M. C. (2022). The intricacies of identifying equatorial waves. *Quarterly Journal of the Royal Meteorological Society*, *148*(747), 2814–2852. doi: 10.1002/qj.4338

Lafore, J.-P., Beucher, F., Peyrillé, P., Diongue-Niang, A., Chapelon, N., Bouniol, D., ... Vischel, T. (2017). A multi-scale analysis of the extreme rain event of ouagadougou in 2009. *Quarterly Journal of the Royal Meteorological Society*, *143*(709), 3094-3109. doi: https://doi.org/10.1002/qj.3165

Laing, A. G., & Fritsch, J. M. (2000). The large-scale environments of the global populations of mesoscale convective complexes. *Monthly Weather Review*, *128*(8), 2756–2776. doi: 10.1175/1520-0493(2000)128⟨2756:TLSEOT⟩2.0.CO;2

Latos, B., Lefort, T., Flatau, M. K., Flatau, P. J., Permana, D. S., Baranowski, D. B., ... Schmidt, J. M. (2021). Equatorial waves triggering extreme rainfall and floods in southwest sulawesi, indonesia. *Mon. Wea. Rev.*, *149*(5), 1381 - 1401. doi: 10.1175/MWR-D-20-0262.1

LeMone, M. A., Zipser, E. J., & Trier, S. B. (1998). The role of environmental shear and thermodynamic conditions in determining the structure and evolution of

mesoscale convective systems during TOGA COARE. *Journal of the Atmospheric Sciences*, *55*(23), 3493–3518. doi: 10.1175/1520-0469(1998)055⟨3493:TROESA⟩2.0.CO;2

Linden, R. v. d., Fink, A. H., Pinto, J. G., Phan-Van, T., & Kiladis, G. N. (2016). Modulation of daily rainfall in southern vietnam by the madden–julian oscillation and convectively coupled equatorial waves. *Journal of Climate*, *29*(16), 5801–5820. doi: 10.1175/JCLI-D-15-0911.1

Lubis, S. W., Hagos, S., Hermawan, E., Respati, M. R., Ridho, A., Risyanto, ... Permana, D. S. (2022). Record-breaking precipitation in indonesia's capital of jakarta in early january 2020 linked to the northerly surge, equatorial waves, and MJO. *Geophysical Research Letters*, *49*(22), e2022GL101513. doi: 10.1029/2022GL101513

Madden, R. A., & Julian, P. R. (1971). Detection of a 40–50 day oscillation in the zonal wind in the tropical pacific. *Journal of the Atmospheric Sciences*, *28*(5), 702–708. doi: 10.1175/1520-0469(1971)028⟨0702:DOADOI⟩2.0.CO;2

Mapes, B. E., & Houze, R. A. (1993). Cloud clusters and superclusters over the oceanic warm pool. *Monthly Weather Review*, *121*(5), 1398–1416. doi: 10.1175/1520-0493(1993)121⟨1398:CCASOT⟩2.0.CO;2

Mapes, B. E., Tulich, S., Lin, J., & Zuidema, P. (2006). The mesoscale convection life cycle: Building block or prototype for large-scale tropical waves? *Dynamics of Atmospheres and Oceans*, *42*(1), 3–29. doi: 10.1016/j.dynatmoce.2006.03.003

Matsuno, T. (1966). Quasi-geostrophic motions in the equatorial area. *J. Meteor. Soc. Japan*, *44*, 25-43. doi: 10.2151/jmsj1965.44.1_25

Mekonnen, A., & Thorncroft, C. D. (2016). On mechanisms that determine synoptic time scale convection over east africa. *International Journal of Climatology*, *36*(12), 4045-4057. doi: doi.org/10.1002/joc.4614

Moncrieff, M. W., Liu, C., & Bogenschutz, P. (2017). Simulation, modeling, and dynamically based parameterization of organized tropical convection for global climate models. *J. Atmos. Sci.*, *74*(5), 1363–1380. doi: 10.1175/JAS-D-16-0166.1

Nakamura, Y., & Takayabu, Y. N. (2022a). Convective couplings with equatorial rossby waves and equatorial kelvin waves. part i: Coupled wave structures. *Journal of the Atmospheric Sciences*, *79*(1), 247–262. doi: 10.1175/JAS-D-21-0080.1

Nakamura, Y., & Takayabu, Y. N. (2022b). Convective couplings with equatorial rossby waves and equatorial kelvin waves. part II: Coupled precipitation characteristics. *Journal of the Atmospheric Sciences*, *79*(11), 2919 – 2933. doi: 10.1175/JAS-D-22-0003.1

Nakazawa, T. (1988). Tropical super clusters within intraseasonal variations over the western pacific. *Journal of the Meteorological Society of Japan. Ser. II*, *66*(6), 823-839. doi: 10.2151/jmsj1965.66.6_823

Nguyen, H., & Duvel, J.-P. (2008). Synoptic wave perturbations and convective systems over equatorial africa. *Journal of Climate*, *21*(23), 6372 - 6388. doi: 10.1175/2008JCLI2409.1

Nicholson, S. E., Fink, A. H., Funk, C., Klotter, D. A., & Satheesh, A. R. (2022). Meteorological causes of the catastrophic rains of october/november 2019 in equatorial africa. *Global and Planetary Change*, *208*, 103687. doi: doi.org/10.1016/j.gloplacha.2021.103687

Ocasio, K. M. N., Evans, J. L., & Young, G. S. (2020). A wave-relative framework analysis of AEW–MCS interactions leading to tropical cyclogenesis. *Monthly Weather Review*, *148*(11), 4657–4671. doi: 10.1175/MWR-D-20-0152.1

Peatman, S. C., Schwendike, J., Birch, C. E., Marsham, J. H., Matthews, A. J., & Yang, G.-Y. (2021). A local-to-large scale view of maritime continent rainfall: Control by ENSO, MJO, and equatorial waves. *Journal of Climate*, *34*(22),

8933–8953. doi: 10.1175/JCLI-D-21-0263.1

Rios-Berrios, R., Judt, F., Bryan, G., Medeiros, B., & Wang, W. (2023). Three-dimensional structure of convectively coupled equatorial waves in aquaplanet experiments with resolved or parameterized convection. *Journal of Climate*, 1–44. doi: 10.1175/JCLI-D-22-0422.1

Rotunno, R., Klemp, J. B., & Weisman, M. L. (1988). A theory for strong, long-lived squall lines. *Journal of Atmospheric Sciences*, *45*(3), 463 - 485. doi: 10.1175/1520-0469(1988)045⟨0463:ATFSLL⟩2.0.CO;2

Roundy, P. E. (2008). Analysis of convectively coupled Kelvin waves in the Indian Ocean MJO. *J. Atmos. Sci.*, *65*, 1342–1359. doi: 10.1175/2007JAS2345.1

Roundy, P. E., & Frank, W. M. (2004). A climatology of waves in the equatorial region. *J. Atmos. Sci.*, *61*(17), 2105–2132. doi: 10.1175/1520-0469(2004)061⟨2105:ACOWIT⟩2.0.CO;2

Rydbeck, A. V., & Maloney, E. D. (2014). Energetics of east pacific easterly waves during intraseasonal events. *Journal of Climate*, *27*(20), 7603–7621. doi: 10.1175/JCLI-D-14-00211.1

Sakaeda, N., Kiladis, G., & Dias, J. (2020). The diurnal cycle of rainfall and the convectively coupled equatorial waves over the maritime continent. *Journal of Climate*, *33*(8), 3307–3331. doi: 10.1175/JCLI-D-19-0043.1

Sakaeda, N., & Torri, G. (2022). The behaviors of intraseasonal cloud organization during DYNAMO/AMIE. *Journal of Geophysical Research: Atmospheres*, *127*(7), e2021JD035749. doi: 10.1029/2021JD035749

Schiro, K. A., Sullivan, S. C., Kuo, Y.-H., Su, H., Gentine, P., Elsaesser, G. S., ... Neelin, J. D. (2020). Environmental controls on tropical mesoscale convective system precipitation intensity. *Journal of the Atmospheric Sciences*, *77*(12), 4233 - 4249. doi: 10.1175/JAS-D-20-0111.1

Schlueter, A., Fink, A. H., & Knippertz, P. (2019). A systematic comparison of tropical waves over northern Africa. Part II: Dynamics and thermodynamics. *J. Climate*. doi: 10.1175/JCLI-D-18-0651.1

Schlueter, A., Fink, A. H., Knippertz, P., & Vogel, P. (2018). A Systematic Comparison of Tropical Waves over Northern Africa. Part I: Influence on Rainfall. *J. Climate*, *32*, 1501–1523. doi: 10.1175/JCLI-D-18-0173.1

Schreck III, C. J. (2021). Global survey of the mjo and extreme precipitation. *Geophysical Research Letters*, *48*(19), e2021GL094691. doi: https://doi.org/10.1029/2021GL094691

Schumacher, C., & Houze, R. A. (2006). Stratiform precipitation production over sub-saharan africa and the tropical east atlantic as observed by TRMM. *Quarterly Journal of the Royal Meteorological Society*, *132*(620), 2235–2255. doi: 10.1256/qj.05.121

Schumacher, R. S., & Johnson, R. H. (2005). Organization and environmental properties of extreme-rain-producing mesoscale convective systems. *Monthly Weather Review*, *133*(4), 961–976. doi: 10.1175/MWR2899.1

Schumacher, R. S., & Rasmussen, K. L. (2020). The formation, character and changing nature of mesoscale convective systems. *Nature Reviews Earth & Environment*, *1*(6), 300–314. doi: 10.1038/s43017-020-0057-7

Serra, Y. L., Rowe, A., Adams, D. K., & Kiladis, G. N. (2020). Kelvin waves during goamazon and their relationship to deep convection. *Journal of the Atmospheric Sciences*, *77*(10), 3533 - 3550. doi: 10.1175/JAS-D-20-0008.1

Stevens, B., Satoh, M., Auger, L., Biercamp, J., Bretherton, C. S., Chen, X., ... Zhou, L. (2019). DYAMOND: the DYnamics of the atmospheric general circulation modeled on non-hydrostatic domains. *Progress in Earth and Planetary Science*, *6*(1), 61. doi: 10.1186/s40645-019-0304-z

Straub, K. H., & Kiladis, G. N. (2003). Interactions between the Boreal Summer Intraseasonal Oscillation and Higher-Frequency Tropical Wave Activity. *Mon. Wea. Rev.*, *131*, 945–960. doi: 10.1175/1520-0493(2003)131⟨0945:IBTBSI⟩2.0

.CO;2

Tabari, H. (2020). Climate change impact on flood and extreme precipitation increases with water availability. *Scientific Report*, *10*(1), 13768. doi: 10.1038/s41598-020-70816-2

Takayabu, Y. N., & Nitta, T. (1993). 3-5 day-period disturbances coupled with convection over the tropical pacific ocean. *Journal of the Meteorological Society of Japan. Ser. II*, *71*(2), 221–246. doi: 10.2151/jmsj1965.71.2_221

Taylor, C. M., Belušić, D., Guichard, F., Parker, D. J., Vischel, T., Bock, O., ... Panthou, G. (2017). Frequency of extreme sahelian storms tripled since 1982 in satellite observations. *Nature*, *544*(7651), 475–478. doi: 10.1038/nature22069

Vasconcelos Junior, F. d. C., Jones, C., Gandu, A. W., & Martins, E. S. P. R. (2021). Impacts of the madden-julian oscillation on the intensity and spatial extent of heavy precipitation events in northern northeast brazil. *International Journal of Climatology*, *41*(6), 3628-3639. doi: https://doi.org/10.1002/joc.7039

Vizy, E. K., & Cook, K. H. (2022). Distribution of extreme rainfall events and their environmental controls in the west african sahel and soudan. *Climate Dynamics*, *59*, 997–1026. doi: doi.org/10.1007/s00382-022-06171-x

Wheeler, M., & Kiladis, G. N. (1999). Convectively coupled equatorial waves: Analysis of clouds and temperature in the wavenumber–frequency domain. *J. Atmos. Sci.*, *56*, 374–399. doi: 10.1175/1520-0469(1999)056⟨0374:CCEWAO⟩2.0.CO;2

Wheeler, M. C., & Hendon, H. H. (2004). An all-season real-time multivariate MJO index: Development of an index for monitoring and prediction. *Mon. Wea. Rev.*, *132*, 1917–1932. doi: 10.1175/1520-0493(2004)132⟨1917:AARMMI⟩2.0.CO;2

Wolding, B., Dias, J., Kiladis, G., Maloney, E., & Branson, M. (2020). Interactions between moisture and tropical convection. part ii: The convective coupling of equatorial waves. *Journal of the Atmospheric Sciences*, *77*(5), 1801 - 1819. doi: 10.1175/JAS-D-19-0226.1

Yasunaga, K., & Mapes, B. (2011a). Differences between more divergent and more rotational types of convectively coupled equatorial waves. part II: Composite analysis based on space–time filtering. *Journal of the Atmospheric Sciences*, *69*(1), 17–34. doi: 10.1175/JAS-D-11-034.1

Yasunaga, K., & Mapes, B. (2011b). Differences between more divergent and more rotational types of convectively coupled equatorial waves. part I: Space–time spectral analyses. *Journal of the Atmospheric Sciences*, *69*(1), 3–16. doi: 10.1175/JAS-D-11-033.1

Ying, Y., & Zhang, F. (2017). Practical and intrinsic predictability of multiscale weather and convectively coupled equatorial waves during the active phase of an mjo. *J. Atmos. Sci.*, *74*, 3771–3785.

Zhang, C. (2005). Madden-julian oscillation. *Reviews of Geophysics*, *43*(2), RG2003. doi: 10.1029/2004RG000158

Supporting Information for "Mesoscale convective systems modulated by convectively coupled equatorial waves"

Yuan-Ming Cheng[1], Juliana Dias[1], George Kiladis[1], Zhe Feng[2], L. Ruby Leung[2]

[1]NOAA/Physical Sciences Laboratory, Boulder, Colorado

[2]Atmospheric Sciences and Global Change Division, Pacific Northwest National Laboratory, Richland, Washington

Contents of this file

1. Figures S1 to S7

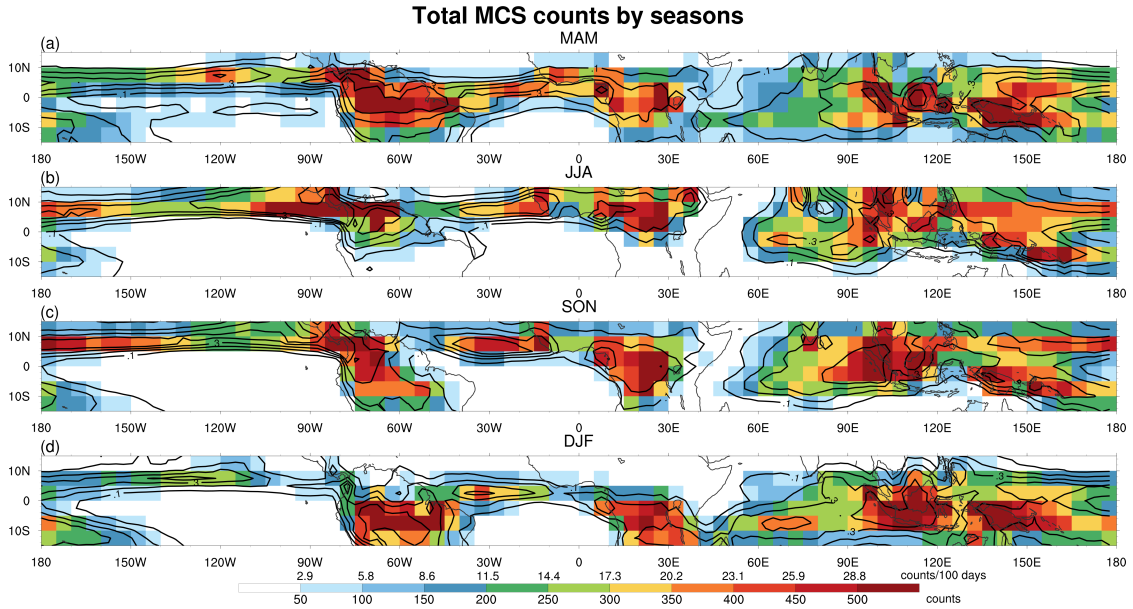

Figure S1. As in Fig. 1a, MCS counts binned in 5° × 5° grid boxes from 2001 to 2019 but for four seasons: (a) MAM, (b) JJA, (c) SON, and (d) DJF. Each MCS is binned by its average lifetime location. Mean seasonal precipitation is contoured at 0.1 mm hr^{-1}.

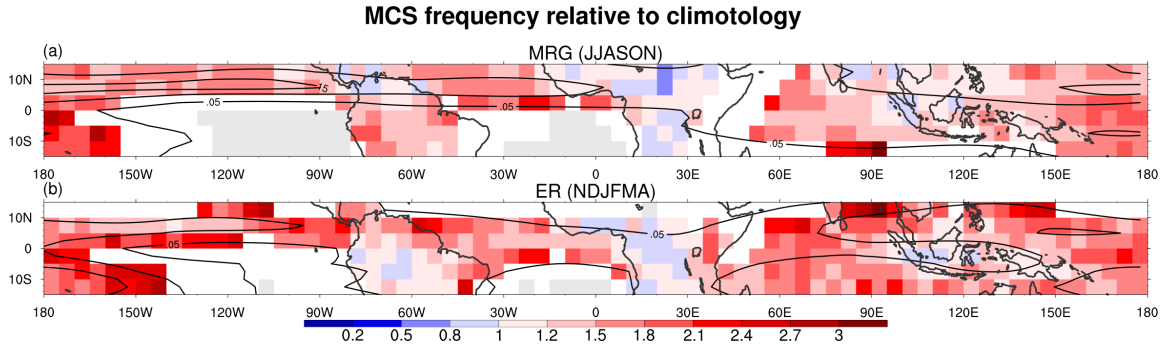

Figure S2. As in Fig. 1b-1d, frequency ratio (R_{freq}, colors) of MCS occurrence relative to climatology when the calculation is conditioned on (a) mixed Rossby gravity waves (MRGs) in JJASON, and (b) equatorial Rossby waves (ERs) in NDJFMA. The mean standard deviation of wave-filtered rainfall in the respective months is contoured every 0.05 mm hr^{-1} with zero lines omitted.

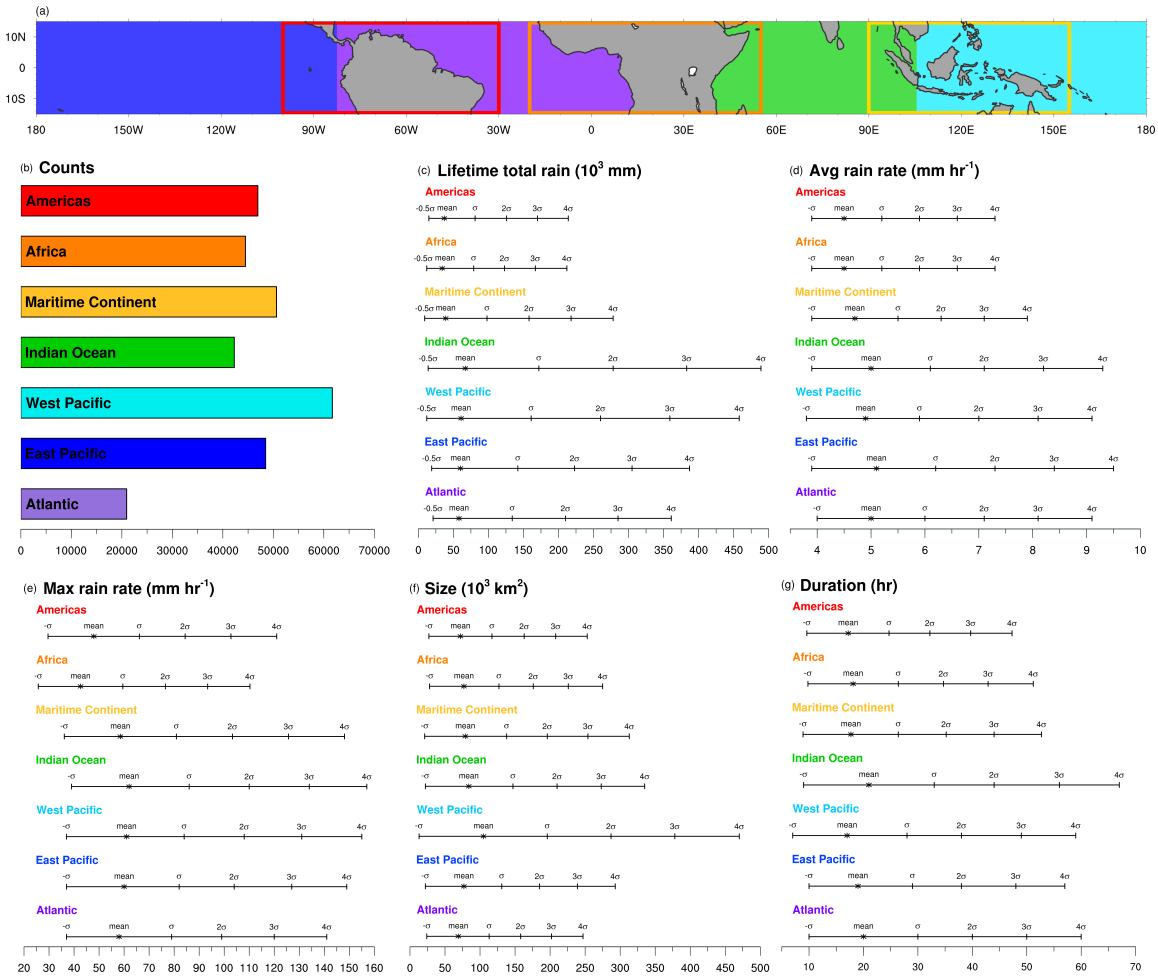

Figure S3. (a) Delineated regions for (b) total MCS counts and (c)–(g) physical quantities of MCS characteristics corresponding to the Z-scores. In (a), boxes denote land regions where all quantities are calculated only over land: the Americas (red), Africa (orange), and Maritime Continent (yellow). Shaded areas show oceanic regions where all values are calculated only over the ocean: Indian Ocean (green), West Pacific (cyan), East Pacific (blue), and Atlantic (purple). In (b), MCS counts are calculated in each region during 2001–2019. In (c)–(g), distributions of physical values are shown in terms of the mean (*) and standard deviation (σ). Lifetime total rain has a unit of 10^3 mm, average rain rate mm hr^{-1}, maximum rain rate mm hr^{-1}, duration hr, and size 10^3 km^2.

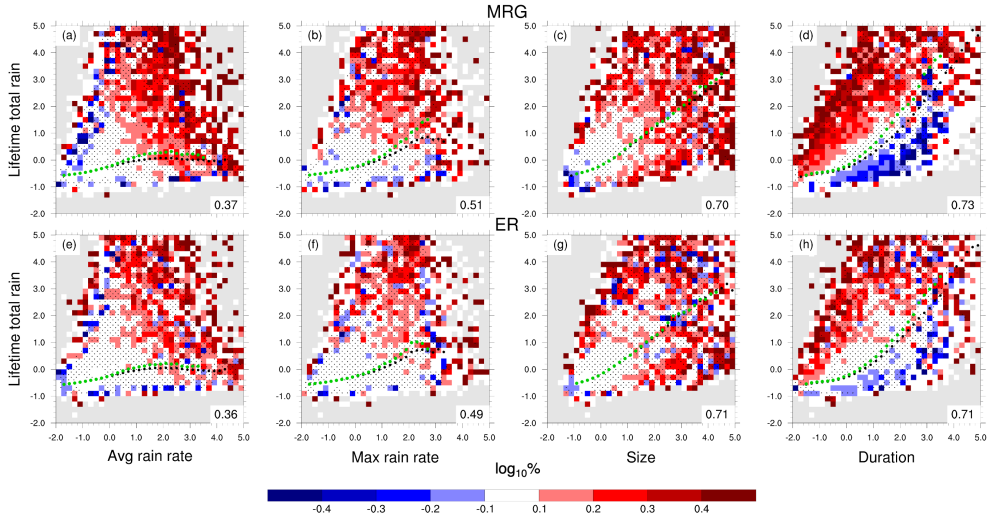

Figure S4. As in the bottom 3 rows of Fig. 2, change of pdfs from all-MCS ones when MCSs are conditioned on (a–d) MRGs, and (e–h) ERs. The first column shows pdfs for average rain rate vs. lifetime total rain; the second maximum rain rate vs. lifetime total rain; the third size vs. lifetime total rain; the fourth duration vs. lifetime total rain. Colors show the log_{10} percentage change from all-MCS pdfs. Numbers on the lower-right corner of each panel denote the correlation coefficient between the two variables for MCS conditioned on CCEWs. Black dots denote the median of lifetime total rain binned by the four characteristics in the x-axis for all MCSs and green dots mark the same median but for CCEW-conditioned MCSs. Stippling shows signals that are statistically *not* significant from the all-MCS pdf at the 95% interval estimated using 1000 times random sampling. Gray shading indicates bins with zero MCS occurrence.

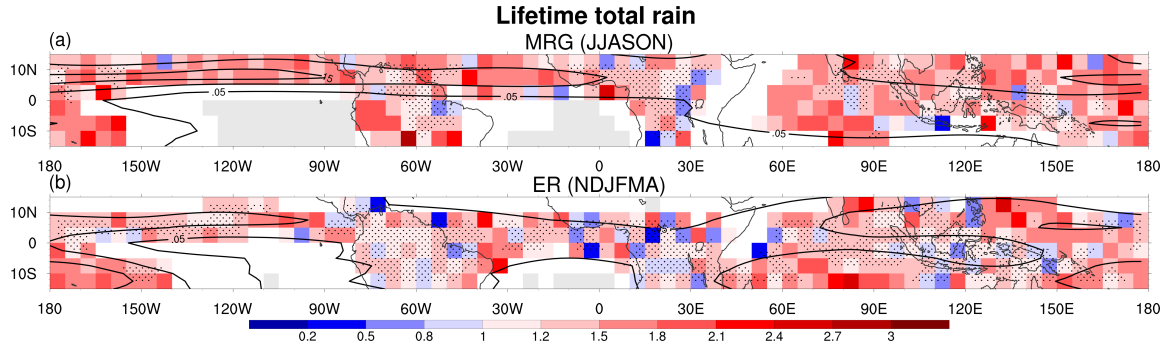

Figure S5. As in Fig. 3a–b, risk ratio (R_{risk}) for extremely high lifetime total rain but for (a) MRGs, and (b) ERs. Mean standard deviation of wave-filtered rainfall in the respective 6 months is contoured every 0.05 mm hr^{-1}. Stippling marks statistically *not* significant regions at the 95% interval estimated using 1000 times random sampling. Grid boxes accumulating less than 100 counts of MCSs over the respective 6 months during 2001–2019 are plotted white and those with no MCS occurrence gray.

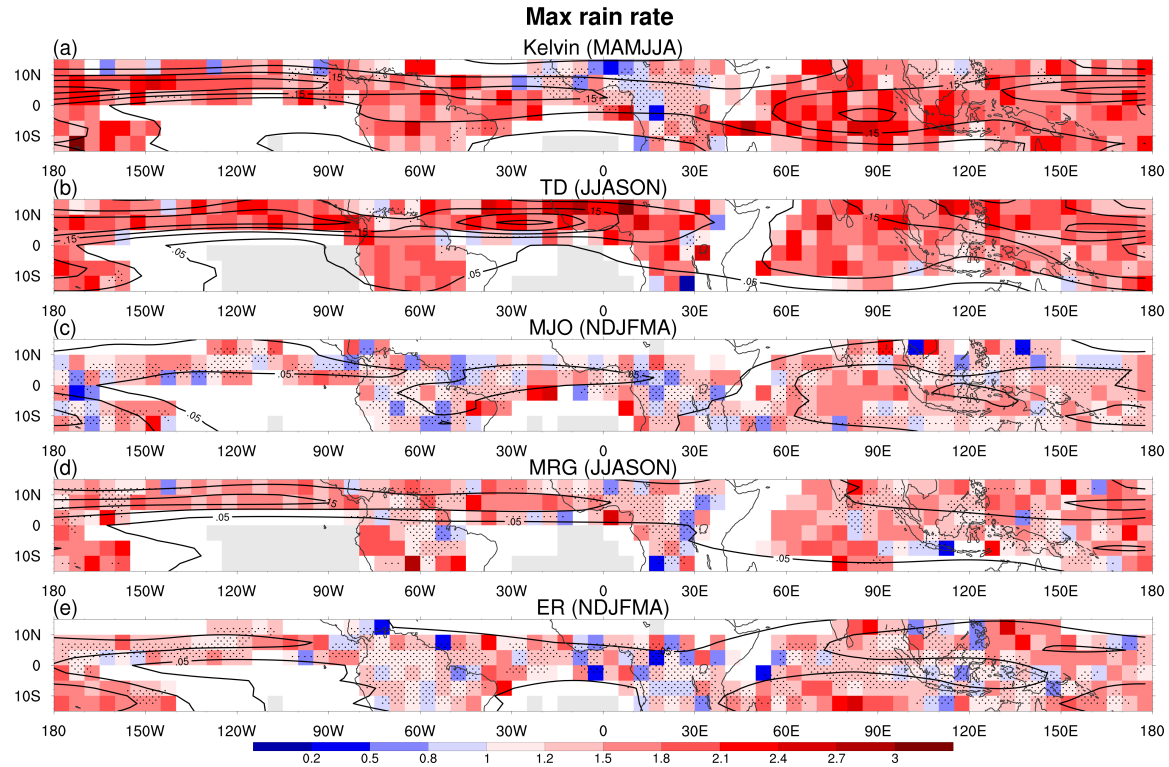

Figure S6. As in Fig. 3a–b, but risk ratio (R_{risk}) for extreme maximum rain rate for (a) Kelvin waves, (b) TDs, (c) the MJO, (d) MRGs, and (e) ERs. Mean standard deviation of wave-filtered rainfall in the respective 6 months is contoured every 0.05 mm hr^{-1}. Stippling marks statistically *not* significant regions at the 95% interval estimated using 1000 times random sampling. Grid boxes accumulating less than 100 counts of MCSs over the respective 6 months in 2001–2019 are shaded white and those with no MCS occurrence gray.

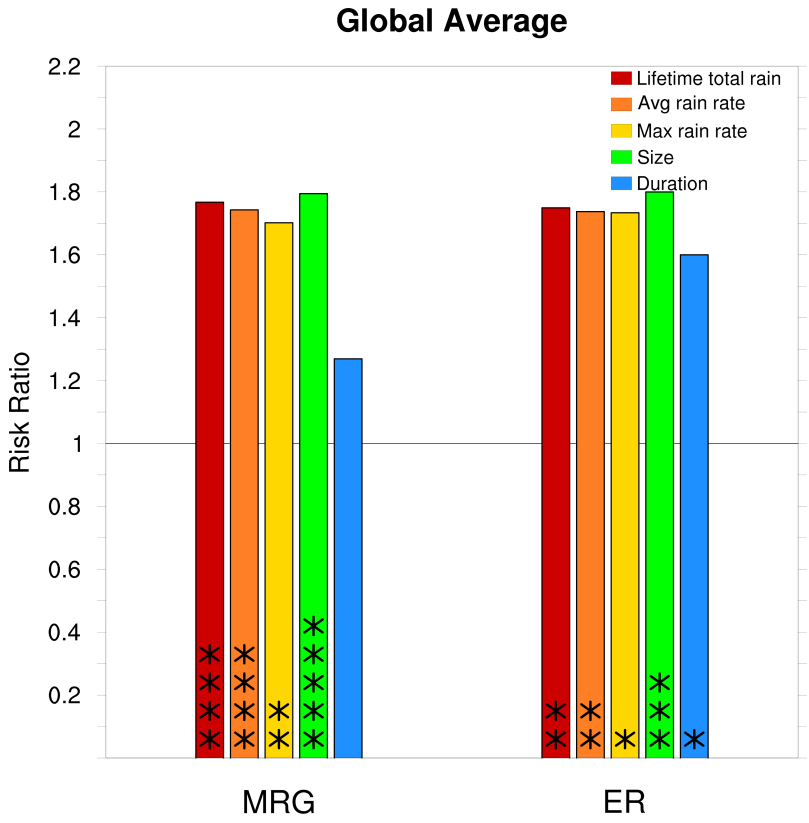

Figure S7. As in Fig. 3d, but global average R_{risk} for MRGs and ERs over the tropics where the risk ratio is statistically significant at the 95% interval. Asterisks indicate how prevalent statistically significant signals are. Each asterisk represents 10% of the grid boxes in the global tropics. The legend shows different flavors of extreme MCSs in various colors.